nagra National Cooperative for the Disposal of Radioactive Waste

TECHNICAL REPORT 91-33

GRIMSEL TEST SITE

MIGRATION EXPERIMENT

MODELLING OF LABORATORY HIGH-PRESSURE INFILTRATION EXPERIMENTS

P.A. SMITH FEBRUARY 1992

PSI, Würenlingen and Villigen

Hardstrasse 73, CH-5430 Wettingen/Switzerland, Telephone + 41-56-37 11 11

nagra National Cooperative for the Disposal of Radioactive Waste

TECHNICAL REPORT 91-33

GRIMSEL TEST SITE

MIGRATION EXPERIMENT

MODELLING OF LABORATORY HIGH-PRESSURE INFILTRATION EXPERIMENTS

P.A. SMITH FEBRUARY 1992

PSI, Würenlingen and Villigen

Hardstrasse 73, CH-5430 Wettingen/Switzerland, Telephone +41-56-37 11 11

FOREWORD

Concepts for the disposal of radioactive waste in geological formations place a significant emphasis on acquiring extensive knowledge of the proposed host rock and the surrounding strata. For this reason, Nagra has, since May 1984, been operating the **Grimsel Test Site (GTS)** which is located at a depth of 450 m in the crystalline rock of the Aare Massif of the Central Swiss Alps. The general objectives of the research being carried out in this underground laboratory include

- the build-up of know-how in planning, performing and interpreting field experiments in various scientific and technical disciplines and

- the acquisition of practical experience in the development of investigation methodologies, measuring techniques and test equipment which will be of use during actual repository site explorations.

The GTS is operated by Nagra and, on the basis of a German-Swiss co-operative agreement, various experiments are carried out by Nagra, the "Bundesanstalt für Geowissenschaften und Rohstoffe, Hannover" (BGR) and the "Forschungszentrum für Umwelt und Gesundheit, München" (GSF). The Grimsel projects of both GSF and BGR are supported by the German Federal Ministry for Research and Technology (BMFT). NTB 85-46 (German version NTB 85-47) provide an overview of the German-Swiss investigation programme. In a special issue of the Nagra Bulletin 1988 (German version "Nagra Informiert 1+2/1988") the status of the programme up to 1988 is described.

The **Radionuclide Migration Experiment (MI)** is the most significant contribution from Nagra to the Grimsel programme. MI is a multidisciplinary study aimed at investigating solute transport in fractured media. Extensive field work is complemented by a substantial programme of hydrodynamic, chemical and transport modeling, along with supporting laboratory studies. This project, initiated in 1985 and currently planned to be terminated in 1994, was initially conceived as a collaborative project between Nagra and the Paul Scherrer Institute (PSI). Since 1987, radiotracer field tests have also been carried out with the Institute of Hydrology of GSF Munich-Neuherberg. In 1989 a bilateral collaboration agreement was signed with the Japanese Power Reactor and Nuclear Fuel Development Corporation (PNC) and the support under this cooperation resulted in a substantial extension of the project.

This report, issued simultaneously as Nagra NTB and PSI Report #117, was produced in accordance with the cooperation agreements mentioned above. The authors have presented their own opinions and conclusions which do not necessarily coincide with those of Nagra or its participating partners.

VORWORT

Bei Konzepten, welche die Endlagerung radioaktiver Abfälle in geologischen Formationen vorsehen, ist die Kenntnis des Wirtgesteins und der angrenzenden Gesteinsschichten von grundlegender Bedeutung. Die Nagra betreibt deshalb seit Mai 1984 das **Felslabor Grimsel (FLG)** in 450 m Tiefe im Kristallin des Aarmassivs. Die generelle Zielsetzung für die Arbeiten in diesem System von Versuchsstollen umfasst

- den Aufbau von Know-how in der Planung, Ausführung und Interpretation von Untergrundversuchen in verschiedenen wissenschaftlichen und technischen Fachgebieten, und

- den Erwerb praktischer Erfahrung in der Entwicklung und der Anwendung von Untersuchungsmethoden, Messverfahren und Messgeräten, die für die Erkundung von potentiellen Endlagerstandorten in Frage kommen.

Im Felslabor der Nagra werden, auf der Basis eines deutsch-schweizerischen Zusammenarbeitsvertrages, verschiedene Versuche von den beiden deutschen Partnern Bundesanstalt für Geowissenschaften und Rohstoffe, Hannover (BGR) und Forschungszentrum für Umwelt und Gesundheit GmbH, München (GSF) durchgeführt. Das Deutsche Bundesministerium für Forschung und Technologie (BMFT) fördert die Arbeiten der BGR und der GSF im FLG. Der NTB 85-47 (englische Version NTB 85-46) enhält eine Uebersicht des FLG und die Zusammenfassung der Untersuchungsprogramme mit Status August 1985. In der Ausgabe 1+2/1988 des Heftes "Nagra informiert" bzw. der englischen Spezialausgabe "Nagra Bulletin 1988" ist der Stand der Arbeiten anfangs 1988 beschrieben.

Der **Migrationsversuch (MI)** ist ein sehr wesentlicher Beitrag zum Grimsel Programm. MI ist ein multidisziplinäres Experiment zur Untersuchung des Transportverhaltens von Radionukliden im Grundwasser eines geklüftetem Gesteins. Die ausgedehnten Feldversuche werden unterstützt durch ein umfangreiches Programm zur hydrodynamischen und chemischen Charakterisierung des MI-Bereichs und zur Modellierung der Transportprozesse sowie durch ergänzende Laboruntersuchungen. Das 1985 begonnene und, gemäss jetziger Planung, bis 1994 dauernde Projekt MI war ursprünglich als gemeinsames Vorhaben der Nagra und des Paul Scherrer Instituts (PSI) konzipiert worden. Seit 1987 führt das Institut für Hydrologie der GSF, München-Neuherberg die Radiotracer-Analysen bei den Feldversuchen durch. Im Jahre 1989 unterzeichnete dann Nagra mit der japanischen Power Reactor and Nuclear Fuel Corporation (PNC) einen Vertrag zur Beteiligung der PNC am Migrationsversuch, wodurch eine wesentliche Erweiterung des Untersuchungsprogrammes ermöglicht wurde.

Der vorliegende Bericht erscheint gleichzeitig als Nagra NTB und als PSI Bericht Nr. 117 und wurde im Rahmen der erwähnten Zusammenarbeitsverträge erstellt. Die Autoren haben ihre eigenen Ansichten und Schlussfolgerungen dargelegt. Diese müssen nicht unbedingt mit denjenigen der Nagra oder der beteiligten Partner übereinstimmen.

AVANT - PROPOS

Lors d'études de concepts de stockage de déchets radioactifs dans des formations géologiques, on attache une grande importance à l'acquisition d'informations étendues sur la roche d'accueil et les formations rocheuses environnantes. C'est pour cette raison que la Cédra exploite depuis mai 1984 son **laboratoire souterrain du Grimsel (LSG)** situé à 450 m de profondeur dans le cristallin du massif de l'Aar, situé au milieu des Alpes centrales. Les principaux objectifs des recherches effectuées dans ce réseau de galeries comprennent:

- l'acquisition de savoir-faire dans diverses disciplines techniques et scientifiques en ce qui concerne la conception, la réalisation et l'interprétation d'expériences in situ, ainsi que

- l'accumulation d'expériences pratiques dans la mise au point et l'application de méthodes d'investigation, de techniques et d'appareillages de mesure, qui pourraient être utilisés lors de l'exploration de sites potentiels de dépôts finals.

Le LSG est exploité par la Cédra et diverses expériences y sont réalisées par celle-ci et deux institutions allemandes: la "Bundesanstalt für Geowissenschaften und Rohstoffe, Hanovre" (BGR) et le "Forschungszentrum für Umwelt und Gesundheit GmbH, Münich" (GSF) dans le cadre d'un traité de collaboration germano-suisse. Les projets poursuivis au Grimsel par la BGR et le GSF sont financés par le Ministère fédéral allemand de la recherche et de la technologie (BMFT). Les rapports NTB 85-46 (version anglaise) et NTB 85-47 (version allemande) présentent un aperçu du laboratoire souterrain et un résumé des programmes de recherches avec état au mois d'août 1985. L'état d'avancement de ce programme en 1988 est présenté dans la publication "Cédra informe 1+2/1988" (version française) et "Nagra informiert 1+2/1988" (version allemande), ainsi que dans une édition spéciale en anglais (Nagra Bulletin 1988).

L'expérience de migration de radionucléides (MI) représente la contribution essentielle de la Cédra au programme du Grimsel. MI est une étude multidisciplinaire ayant pour objectif l'étude du transport en solution en milieu fissuré. Les travaux de terrain intensifs sont complétés par un programme de modélisation hydrodynamique, chimique et de transport, ainsi que par des essais en laboratoire. Ce projet, qui a débuté en 1985 et devrait se terminer en 1994, fut initialement conçu comme une collaboration entre la Cédra et l'Institut Paul Scherrer (IPS). Depuis 1987 des essais de terrain avec des traceurs radioactifs ont été réalisés par l'institut d'hydrologie de la GSF de Munich-Neuherberg. En 1989 un accord bilatéral de collaboration a été signé avec la "Power Reactor and Nuclear Fuel Development Corporation" (PNC) du Japon qui a conduit à une extension substantielle du programme d'investigation.

Le présent rapport, publié simultanément en tant que rapport technique Cédra (NTB) et rapport IPS N° 117, a été élaboré dans le cadre des accords de collaboration mentionnés. Les auteurs ont présenté leurs vues et conclusions personnelles. Celles-ci ne doivent pas forcément correspondre à celles de la Cédra ou à celles de ses partenaires participants.

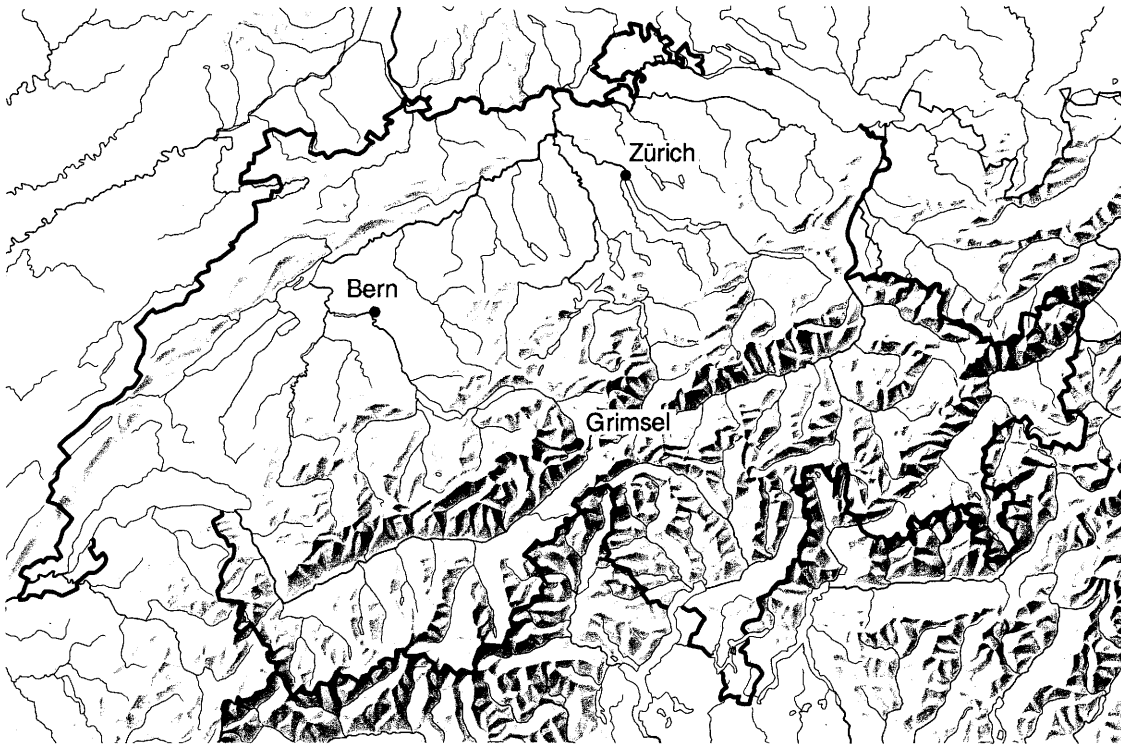

Location of Nagra's underground test facility at the Grimsel Pass in the Central Alps (Bernese Alps) of Switzerland (approximate scale 1 cm = 25 km).

Geographische Lage des Nagra Felslabors am Grimselpass (Berner Oberland) in den schweizerischen Zentralalpen (Massstab: 1 cm = ca. 25 km)

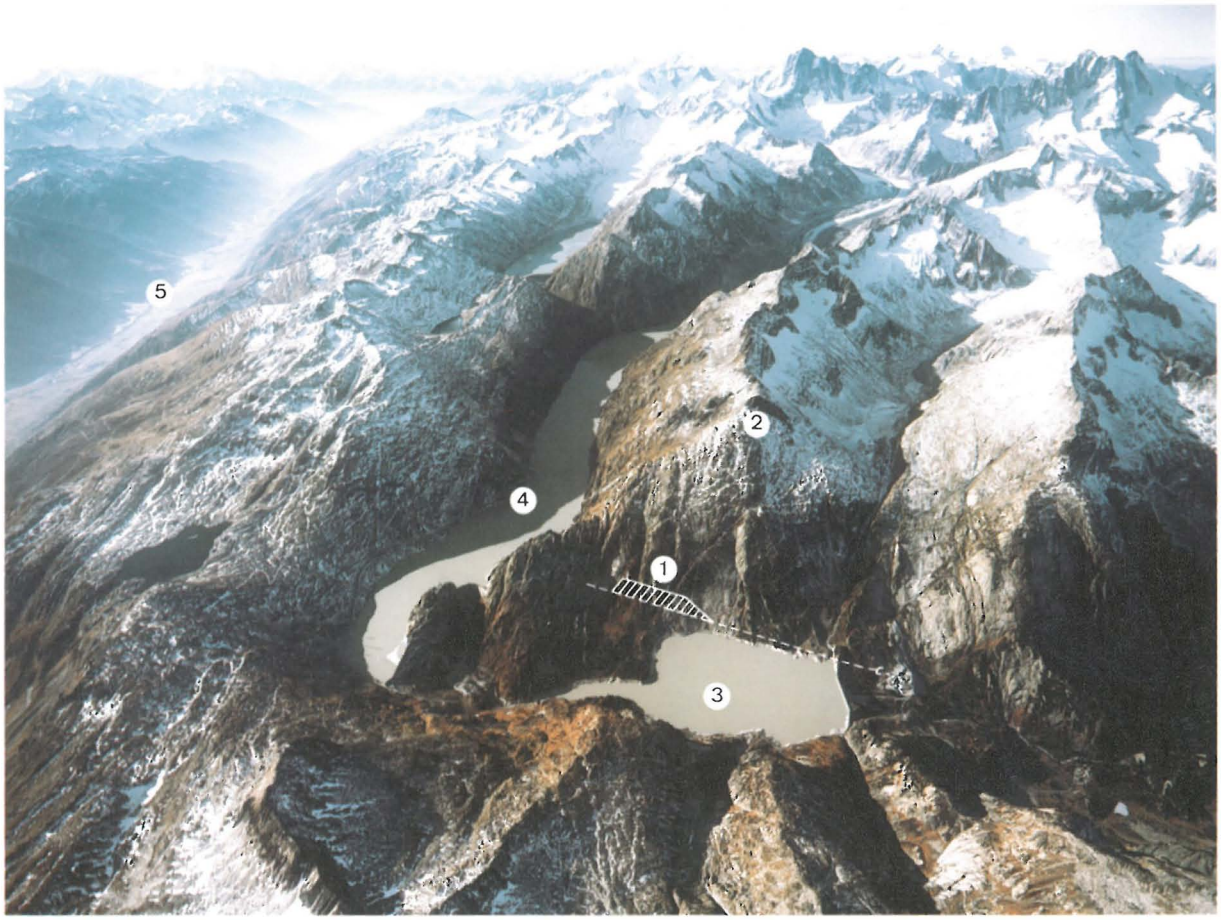

GRIMSEL-GEBIET

Blick nach Westen

1 Felslabor
2 Juchlistock
3 Räterichsbodensee
4 Grimselsee
5 Rhonetal

GRIMSEL AREA

View looking West

1 Test Site
2 Juchlistock
3 Lake Raeterichsboden
4 Lake Grimsel
5 Rhone Valley

FLG FELSLABOR GRIMSEL
GTS *GRIMSEL TEST SITE*

Situation

0 100 m

- Zugangsstollen/*Access tunnel*
- Fräsvortrieb/*by tunnel boring machine*
- Sprengvortrieb/*excavated by blasting*
- Zentraler Aaregranit ZAGR / *Central Aaregranite CAGR*
- Biotitreicher ZAGR / *CAGR with high content of biotite*
- Grimsel-Granodiorit / *Grimsel-Granodiorite*
- Scherzone/*Shear zone*
- Lamprophyr/*Lamprophyre*
- Wasserzutritt/*Water inflow*
- SB Sondierbohrung/*Exploratory borehole*
- US US Bohrung/*US borehole*

ZB	Zentraler Bereich/*Central facilities*
AU	Auflockerung/*Excavation effects*
BK	Bohrlochkranz/*Fracture system flow*
EM	El.magn. HF-Messungen/*-measurements*
FRI	Kluftzone/*Fracture zone investigation*
GS	Gebirgsspannungen/*Rock stresses*
HPA	Hydr. Parameter/*Hydr. parameters*
MI	Migration/*Migration*
MOD	Hydrodyn. Modellierung/*H. modeling*
NM	Neigungsmesser/*Tiltmeters*
UR	Untertageradar/*Underground radar*
US	Seismik/*Underground seismic testing*
VE	Ventilationstest/*Ventilation test*
WT	Wärmeversuch/*Heat test*

A — A Schnitt/*Section*

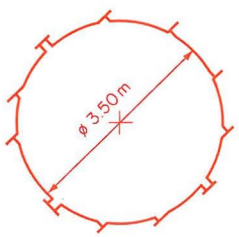

6/88

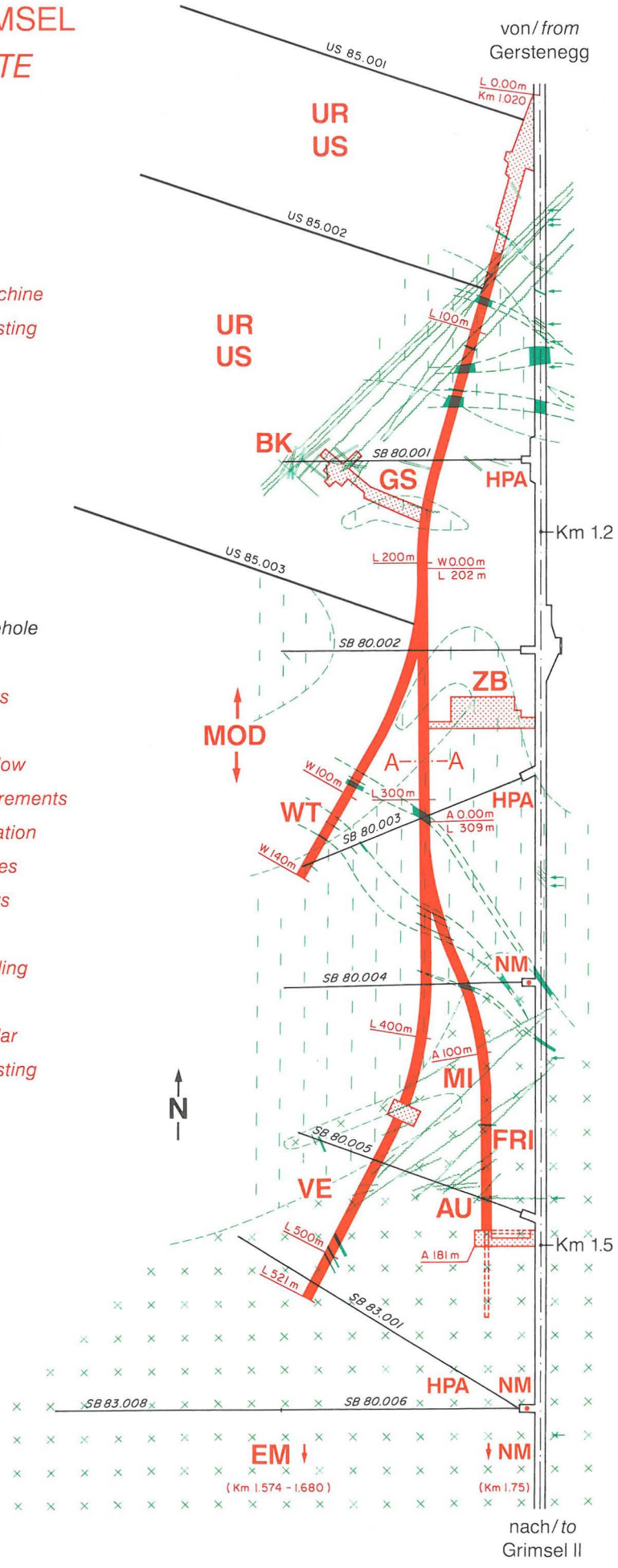

Contents

Abstract

This report describes the modelling of break–through curves from a series of two–tracer dynamic infiltration experiments, which are intended to complement larger scale experiments at the Nagra Grimsel Test Site. The tracers are ^{82}Br, which is expected to be non–sorbing, and ^{24}Na, which is weakly sorbing. The ^{24}Na concentration is well below the natural Na concentration in the infiltration fluid, so that sorption on the rock is governed by isotopic exchange, exhibiting a linear isotherm. The rock specimens are sub–samples (cores) of granodiorite from the Grimsel Test Site, each containing a distinct shear zone. Best–fits to the break–through curves using single–porosity and dual–porosity transport models are compared and several physical parameters are extracted. It is shown that the dual–porosity model is required in order to reproduce the tailing part of the break–through curves for the non–sorbing tracer. The single–porosity model is sufficient to reproduce the break–through curves for the sorbing tracer within the estimated experimental errors. Extracted K_d values are shown to agree well with a field rock–water interaction experiment and *in situ* migration experiments. Static, laboratory batch–sorption experiments give a larger K_d, but this difference could be explained by the larger surface area available for sorption in the artificially crushed samples used in the laboratory and by a slightly different water chemistry.

Zusammenfassung

In diesem Bericht wird die Modellierung von Durchbruchskurven aus einer Reihe von dynamischen Infiltrationsexperimenten mit zwei Tracern beschrieben. Sie sind als Ergänzung der Migrationsexperimente auf grösserem Massstab im Felslabor Grimsel zu betrachten. Die Tracer sind ^{82}Br, das als nichtsorbierend angenommen wird, und das schwach sorbierende ^{24}Na. Die ^{24}Na-Konzentration liegt erheblich unter der natürlichen Natrium-Konzentration des Infiltrationswassers, sodass die Sorption am Gestein durch Isotopenaustausch bestimmt wird und sich eine lineare Sorptionsisotheme ergibt. Das Gesteinsmaterial besteht aus Bohrkernen aus dem Granodiorit der Migrationszone im Grimsel Felslabor der NAGRA, wobei jeder Bohrkern eine deutliche Scherzone aufweist. Unter Benützung von Transportmodellen einfacher und doppelter Porosität werden Best-Fits an die Durchbruchskurven durchgeführt und mehrere physikalische Parameter bestimmt. Es zeigt sich, dass für den nichtsorbierenden Tracer nur das Modell doppelter Porosität den Schwanz der Durchbruchskurve reproduzieren kann. Innerhalb der geschätzten experimentellen Fehler genügt ein Modell einfacher Porosität, um die Durchbruchskurven des sorbierenden Tracers zu reproduzieren. Die extrahierten K_d-Werte stimmen gut mit solchen aus einem Gesteins-Wasser-Wechselwirkungsexperiment und Migrationsexperimenten im Felslabor überein. Statische Labor-Batchexperimente ergeben grössere Gleichgewichtsverteilungskonstanten für die Sorption. Die Differenz kann jedoch mit einer durch das künstliche Brechen des Gesteins vergrösserten Oberfläche und mit einer leicht unterschiedlichen Wasserchemie in den Batchexperimenten erklärt werden.

1 Introduction

Confidence in a model for the transport of sorbing radionuclides is enhanced by its ability to reproduce experimental data using model parameter values which are consistent with independent measurements. Confidence is further enhanced if the model can reproduce data from a variety of experimental systems which cover differing scales of space and time. For this reason, the large–scale field migration work at the Nagra Grimsel Test Site (GTS) has been complemented by a laboratory–based support programme, including high–pressure infiltration experiments, giving analogous data for small–scale systems, and static batch–sorption experiments, giving independent measurements of sorption properties. This also motivated the selection of small–scale infiltration experiments as a test case in the international INTRAVAL study, the aim of which is the validation of geosphere transport models [1], [2].

Two radionuclide transport models, based on the assumptions of single–porosity and a dual–porosity media, have previously been fitted to break–through curves for both sorbing and non–sorbing radionuclide tracers, measured during infiltration experiments on fractured rock samples from GTS [3]. The single–porosity model accounts for the advection, dispersion and retardation due to sorption on fracture surfaces. The dual–porosity model also accounts for diffusion out of the fractures into a spatially–limited porous zone, referred to as the porous matrix [4].

In principle, the best–fit to the break–through curves allows the goodness–of–fit of the different models to be compared and physical and chemical properties of the rock/water system to be determined. A similar exercise, based on the dual–porosity model, was carried out on data from the migration experiment at GTS, for a series of tests in which the same sorbing tracer was used [5]. Samples for the infiltration experiments were taken from a region of small shear zones branching from the test fracture of the migration experiment and are assumed to be mineralogically (and chemically) similar[1]; a comparison is therefore possible between the sorption properties obtained from modelling the large–scale and small-scale experiments. Comparison can also be made with directly measured values from the batch sorption experiments [6].

However, the results from the infiltration experiments [3] were not sufficiently accu-

[1]There are, however, *structural* differences. In particular, shear zones within the samples for the infiltration experiment lack the infill material of the test fracture. The assumption of *mineralogical* similarity will be investigated in detail in a forthcoming report.

rate to allow all the required information to be extracted from break–through curves for the non–sorbing tracer. As a result, only the product of the diffusion coefficient with the matrix distribution coefficient in the dual–porosity model could be determined, rather than separate values; the range of values extracted for this product was, however, found to be consistent with the distribution coefficient calculated from the results of the migration experiment at GTS.

In order to evaluate the diffusion and sorption parameters of the dual–porosity model separately, further experiments have been performed at the PSI Hotlabor with a modified apparatus and experimental procedure. This report documents the modelling of these new results [7], together with a reworking of earlier data and a comparison of derived physical parameters from this experiment with those from other, independent experiments.

2 Experimental

Two cylindrical rock cores (core 1 and core 2) consisting of granodiorite from the Grimsel Test Site were used in these experiments [2], each containing a distinct mica–rich shear zone formed by ductile displacement during Alpine metamorphism. The cores were extracted at distances of $19.23m$ and $20.38m$ along the drill core BOMI86.004, which intersects the test fracture of the GTS migration experiment at $20.66m$. They were cut from the drill core in such a way that in each case the shear zone lay along the symmetry axis of the core. Cores 1 and 2 are of length $3.05cm$ and $4.38cm$ respectively; both have a diameter of $4.6cm$. A cross section of core 1 is shown in fig. 1a. The experimental methodology can be summarised as follows. Infiltration fluid (natural Grimsel groundwater from the MI fracture) is forced through a core, which is confined within a high–pressure cell. The core is mounted between two stainless steel end–pieces, which are designed to distribute infiltration fluid across the surface of the core on the high–pressure (upstream) side and to collect the emerging fluid on the low–pressure (downstream) side (fig.1b). Once the system has reached a steady state, a pulse containing one or more radioactive tracers is injected into the infiltration fluid and the resulting break–through curves, i.e. the time dependence of the activities of each tracer at the downstream end of the cores, are recorded (fig.2: see [3] and [8] for details).

[2] It is intended to document the samples and methodology of this experiment more comprehensively in a forthcoming report.

It has been shown that the break–through curve for a single sorbing tracer contains insufficient information to enable all physical parameters of interest to be determined uniquely [3]. Therefore, it is first necessary to model the case of a non–sorbing tracer and use the information thus obtained to constrain the model for the sorbing tracer. For this reason, experiments were performed in which both sorbing (^{24}Na) and non–sorbing (^{82}Br) radionuclides were included in the tracer pulse [8]. For this system, the sorption mechanism for Na is cation exchange [9]. The concentration of ^{24}Na is well below that of natural Na in the infiltration fluid, so that sorption on the rock is governed by isotopic exchange and a linear sorption isotherm can be assumed in modelling its transport behaviour. In the original two–tracer experiments, the form of the tracer pulse as it entered the core at the high–pressure side was not well–determined. This was because experimental artifacts (dispersion effects produced by the apparatus) were similar in magnitude to the effects of dispersion and matrix diffusion on the non–sorbing radionuclide in the cores themselves. The latter processes could thus not be separated from the artifacts, seriously limiting the usefulness of the break–through curves. The apparatus and experimental procedure were then modified to allow for these artifacts to be quantified [10]. In the present experiments, a "blank–run" is first carried out, in which the two end–pieces are pressed together with no core present (fig.3a). The break–through curve from the blank–run is taken to give the initial form of the tracer pulse on entry into the cores, which is then used as input when modelling the break–through curves in the presence of the cores (fig.3b), thus incorporating dispersion due to the apparatus into the model (fig.3c).

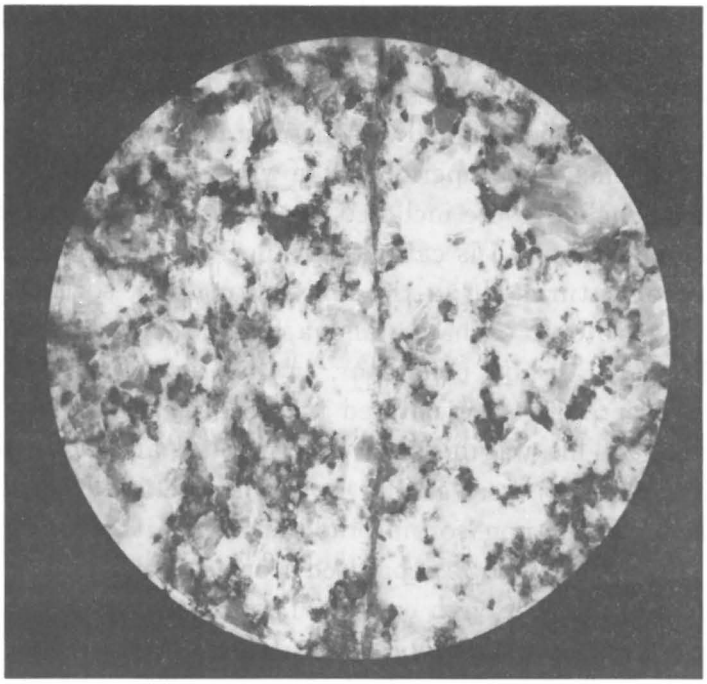

(a) cross section of core

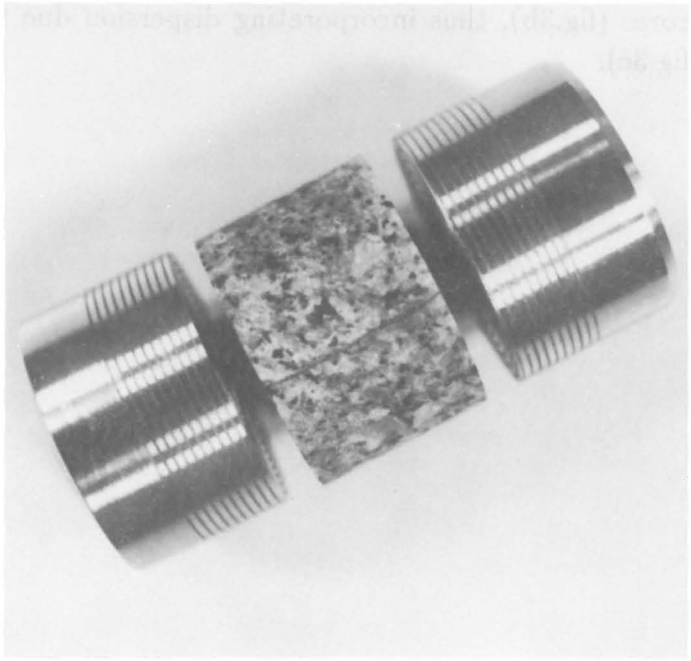

(b) side view, including end pieces

Figure 1: Infiltration core 1 used in experiments BOMI58, BOMI61 and BOMI62.

Diameter of core : 4.6 cm.

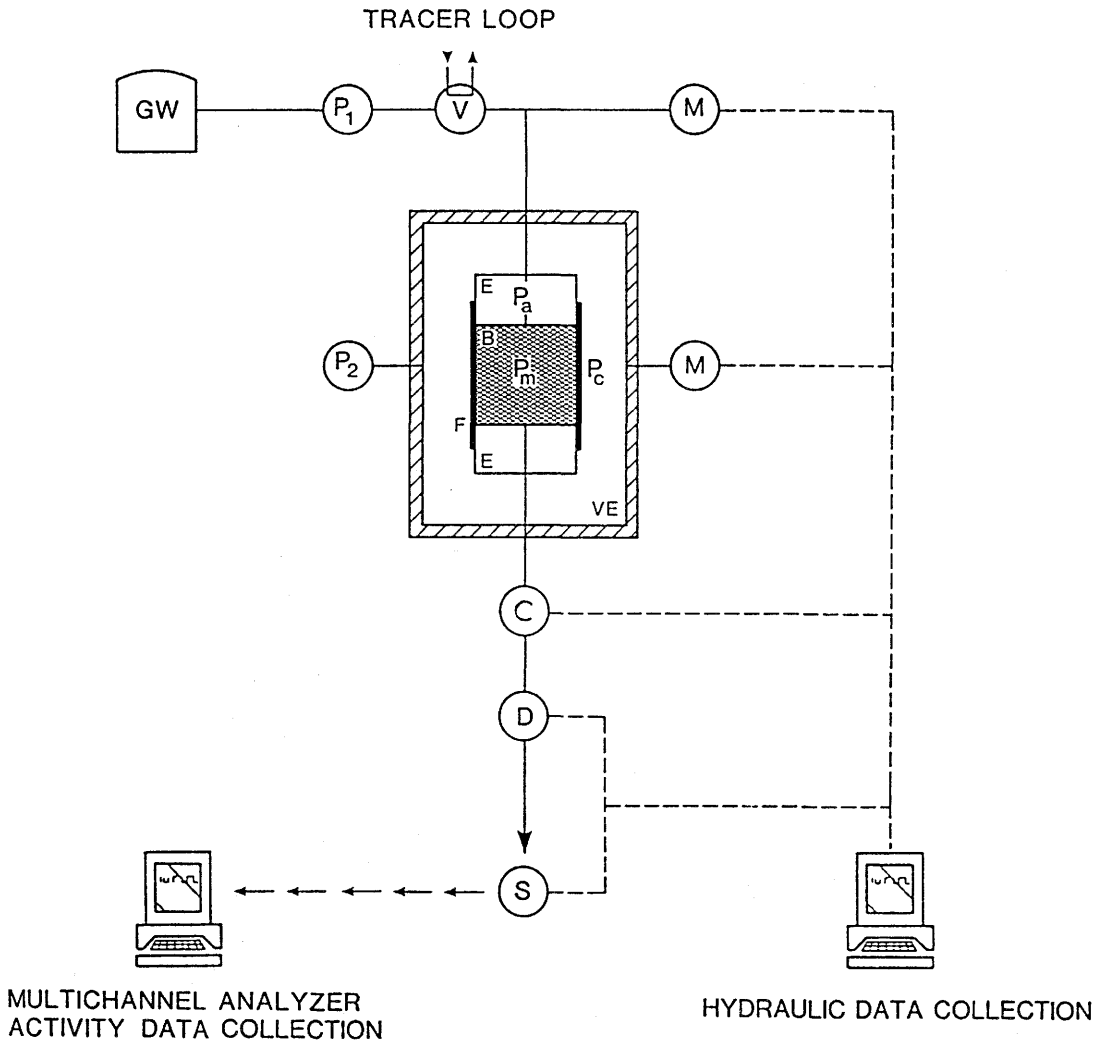

Figure 2. Schematic diagram of the pressure infiltration apparatus.

Core assembly with **B** core sample, **E** end pieces, **F** rubber sleeve.
$\mathbf{P}_1$ infiltration pump, $\mathbf{P}_2$ confining pressure pump,
$\mathbf{P}_c$ confining pressure, $\mathbf{P}_a$ infiltration pressure, $\mathbf{P}_m$ pore pressure,
GW groundwater vessel, **VE** pressure vessel, **V** injection valve,
M manometers and pressure sensors, **C** electrical conductivity sensor,
D droplet counter, **S** fraction/droplet sampler.

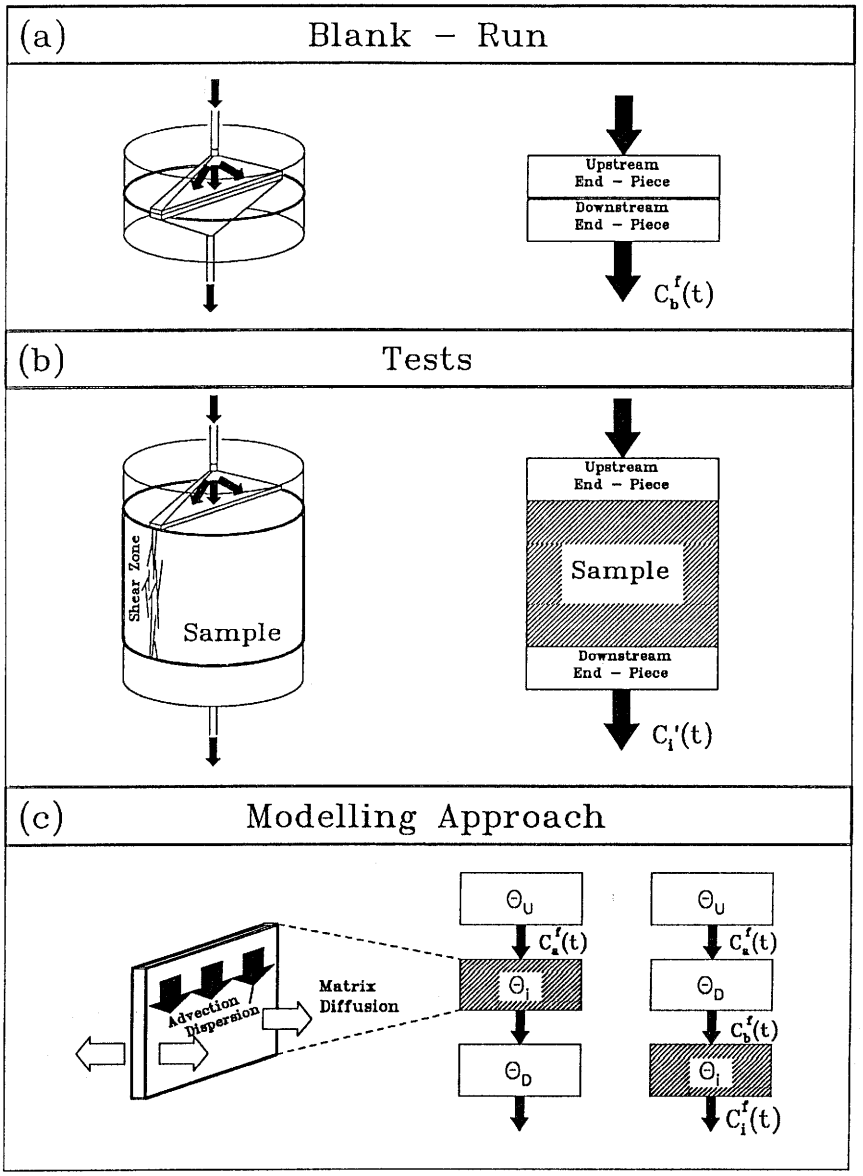

Figure 3. Experimetal procedure and modelling approach.

Artifact generation by the apparatus is taken into account by means of a blank–run.
(a) The blank–run gives a break–through curve $C_b^f(t)$.
(b) The test using tracer i gives a experimental break–through curve $C_i'(t)$.
(c) The transport model gives a calculated break–through curve $C_i(t)$.
Operator Θ_D, representing dowstream end–piece, is commuted with Θ_i, representing the transport model (see section 3), in order that $C_b^f(t)$ provides an input function for the transport model.

3 Modelling of Break–through Curves

3.1 Transport Models

The shear zone through a core is modelled as a single fracture of width (aperture) $2b[m]$ and length $L[m]$ (assumed equal to the length of the core), with an adjacent porous matrix of limited thickness $x_{max\ i}[m]$ for tracer i. $i = 1$ will be used to denote the non–sorbing tracer and $i = 2$ to denote the sorbing tracer. The matrix thickness may vary according to the tracer i when, for example, ionic radius or charge influence matrix diffusion. A Cartesian coordinate system (x, z) is adopted: the z axis is parallel to the direction of fluid flow and the x axis is perpendicular to the plane of the fracture. $z = 0$ is at the inlet of the fracture and $x = 0$ is at its centre. In the dual–porosity model employed here, transport of tracer i along a fracture is described by the following partial differential equations

$$\frac{\partial C_i}{\partial t} = S_i \frac{\partial^2 C_i}{\partial z^2} + T_i \frac{\partial C_i}{\partial z} + U_i \frac{\partial P_i}{\partial x'} |_{x'=0} \tag{1}$$

$$\frac{\partial P_i}{\partial t} = V_i \frac{\partial^2 P_i}{\partial x_i'^2} \; ; \; x_i' \geq 0. \tag{2}$$

$C_i(z,t)[-]$ and $P_i(x_i', t)[-]$ are the concentrations of tracer i in the liquid phase within the fracture and the porous matrix respectively, scaled by the concentration in the injected pulse. $S_i[m^2 s^{-1}]$, $T_i[m s^{-1}]$, $U_i[s^{-1}]$ and $V_i[s^{-1}]$ are tracer–dependent coefficients which are to be determined by fitting the model to the experiments. The transformation

$$x_i' = \frac{x - b}{x_{max\ i}} \tag{3}$$

has been used so that $x_{max\ i}$ appears in neither the governing equations nor the boundary conditions, but is incorporated into the coefficients U_i and V_i.

The terms on the right–hand side of equation (1) represent respectively dispersion and advection within the fracture and the flux of tracer between the fracture and the adjacent porous matrix. Diffusion through the porous matrix is described by equation (2). The single–porosity model is a special case of the dual–porosity model, in which the flux into the matrix is set to zero ($U_i \equiv 0 s^{-1}$) and only equation (1) is solved.

It is assumed that the core is initially free of tracer nuclides, so that

$$C_i(z,t) = 0 \; ; \; \forall z, \; t = 0 \tag{4}$$

$$P_i(x_i', t) = 0 \; ; \; \forall x_i', \; t = 0 \tag{5}$$

$C_b^f(t)[-]$[3] represents the break–through curve from the blank–run; the boundary condition at the inlet to the fracture is obtained by equating the mass flux from the apparatus to the advective *and* dispersive mass fluxes within the fracture

$$C_i(0,t) + \frac{S_i}{T_i}\frac{\partial C_i}{\partial z}(0,t) = C_b^f(t) \; ; \; t > 0 \tag{6}$$

Here, in order to include dispersion in the apparatus into the transport models via C_b^f, the experimental system is modelled as though all parts of the apparatus which influence the form of the break–through curves lie upstream of the core. It is thus assumed that the effects of the downstream end–piece, denoted by an operator Θ_D, may be interchanged with the effects of the core itself, symbolized by an operator Θ_i for the tracer i

$$C_i^f(L,t) = \Theta_D\{\Theta_i[C_a^f(t)]\} = \Theta_i\{\Theta_D[C_a^f(t)]\} = \Theta_i[C_b^f(t)] \tag{7}$$

where $C_a^f(t)$ is the time–dependence of the concentration at the interface between the upstream end–piece and the core. The commutativity of Θ_D and Θ_i can be shown mathematically if the operators are linear [11]. However, it is unclear that the contact with the downstream end–piece is identical in a blank–run and an actual test; no method has as yet been devised to test this experimentally. Future experiments will employ endpieces with negligible dispersion effects, so avoiding this source of uncertainty.

At the outlet

$$\frac{\partial C_i}{\partial z}(L,t) = 0 \; , \; C_i^f(L,t) = C_i(L,t) \; ; \; \forall t \tag{8}$$

describing free flow into the sampler.

Concentration in the liquid phase is continuous across the boundary between the fracture and the matrix

$$C_i(z,t) = P_i(0,t) \; ; \; \forall z, \forall t \tag{9}$$

A zero-gradient condition is imposed at the outer boundary of the porous matrix

$$\frac{\partial P_i}{\partial x_i'}(1,t) = 0 \; ; \; \forall t. \tag{10}$$

The governing equations are solved using code RANCHMD [12]. A set of time dependent, ordinary differential equations is derived from equations (1) and (2) using the Lagrange interpolation technique and integrated by Gear's variable order predictor-corrector method.

[3] the superscript f indicates a *flow–averaged* concentration. The remaining are *resident* concentrations.

3.2 Regression Parameters

There are two independent coefficients for each tracer (S_i and T_i) in the single–porosity model and a further two (U_i and V_i) in the dual–porosity model, each of which is determined by fitting the models to the break–through curves using the non–linear least–squares technique. The χ_i^2 merit function is defined by :

$$\chi_i^2 \equiv \sum_{j=1}^{N_i} \left(\frac{C_i(L, t_{i,j}) - C_i'(t_{i,j})}{\sigma_{i,j}} \right)^2 \tag{11}$$

where $C_i'(t_{i,j})$ is the experimental break–through curve, measured at the N_i times $t_{i,j}, j = 1, N_i$. Each of these data is associated with a measurement error characterised by a standard deviation $\sigma_{i,j}$. $C_i(L, t_{i,j})$ is the tracer concentration at the downstream side of the core ($z = L$), calculated from equations (1) and (2) for a particular set of coefficients. The coefficients may be taken as regression parameters[4] and the merit function is minimised using the Levenberg-Marquardt technique [13]. This procedure yields the best–fit regression parameters, together with their standard errors[5].

For the particular experients considered in this report, the uncertainty to be associated with the data has not been given. However, if it is assumed that all the measurements using a particular tracer are described by a normal distribution, having the same standard deviation (taken as 1, say) **and it is assumed that the model well represents all relevant physical processes**, then the model can be fitted by minimizing χ_i^2 and then σ_i recomputed according to

$$\sigma_i^2 = \frac{\chi_i^2}{N_i} \tag{12}$$

Although this approach allows an error bar to be assigned to the points when measurement error is not known, it also **prohibits an independent assessment of goodness–of–fit** of a particular model. In other words, it cannot objectively be determined whether a particular model does or does not fit the experimental data well. A comparison of χ_i or σ_i does, however, give a measure of the relative goodness–of–fit of the different models to the same set of experimental data.

[4] In practice, $Log_{10}S_i$, $Log_{10}(-T_i)$, $Log_{10}U_i$ and $Log_{10}V_i$ are taken as regression parameters; logarithms are used in order to give each of the regression parameters the same order of magnitude.

[5] It is important to apply the procedure several times using different starting parameters in order to ensure that a unique minimum has been located.

3.3 Physical Parameters

Having obtained the best–fit regression parameters for the two tracers, physical parameters (or combinations of parameters) can then be calculated. There are four in the case of the single–porosity model:

$$a_{Li} = -\frac{S_i}{T_i}, \quad i = 1,2 \tag{13}$$

$$R_f = \frac{T_1}{T_2} \tag{14}$$

$$u = -T_1 \tag{15}$$

and an additional four in the case of the dual-porosity model [6]:

$$\frac{\epsilon_p^2 D_p}{b^2} = \frac{U_1^2}{V_1} \tag{16}$$

$$\frac{\rho_p K_d}{\epsilon_p} \simeq \frac{T_1^2 U_2^2 V_1}{T_2^2 U_1^2 V_2} \tag{17}$$

$$\frac{\epsilon_p x_{max\ 1}}{b} = \frac{U_1}{V_1} \tag{18}$$

$$\frac{\epsilon_p x_{max\ 2}}{b} = \frac{T_2 U_1^2}{V_1 T_1 U_2} \tag{19}$$

Here, $a_{Li}[m]$ is the longitudinal dispersion length for tracer i, $R_f[-]$ is the surface–based retardation factor of the sorbing tracer, $u[ms^{-1}]$ is the velocity of the infiltration fluid and $\epsilon_p[-]$, $\rho_p[m^3kg^{-1}]$, $\epsilon_p D_p[m^2s^{-1}]$ and $K_d[kgm^{-3}]$ are the porosity, density, effective diffusion coefficient and distribution coefficient (for the sorbing tracer) of the porous matrix.

[6] In principle, D_p and ϵ_p could also be tracer dependent

4 Results

Computations were carried out using a uniform rectangular mesh for RANCHMD, with 40 nodes discretising the fracture in the z–direction and 10 nodes discretising the matrix in the x'–direction. Once the models had been fitted to the experimental break–through curves, the sensitivity of the results to mesh refinement was checked. In no case did a refinement of the mesh to 60 nodes in the z–direction and 24 nodes in the x'–direction result in a change of more than 2% in χ_i^2.

Tables 1 and 2 present the regression parameters extracted from 5 experiments on the two cores using the single–porosity and dual–porosity transport models respectively. The errors given in the tables correspond to one standard deviation in the various regression parameters. The physical parameters, derived using equations (13-19), are presented in tables 3 and 4. Experiments BOMI58, BOMI61 and BOMI62 were performed on core 1, while BOMI60 and BOMI69 were performed on core 2. BOMI58, BOMI61 and BOMI62 were carried out using practically the same

	core 1			*core 2*		
	BOMI58	**BOMI61**	**BOMI62**	**BOMI60**	**BOMI69N**	**BOMI69Z**
$-Log_{10}(S_1)$	a)	7.32 ± 0.01	7.46 ± 0.02	a)	6.45 ± 0.01	6.17 ± 0.02
$-Log_{10}(-T_1)$	a)	4.855 ± 0.002	4.846 ± 0.003	a)	4.964 ± 0.003	4.948 ± 0.004
$-Log_{10}(S_2)$	7.59 ± 0.01	7.64 ± 0.01	7.72 ± 0.01	7.750 ± 0.007	7.93 ± 0.02	7.90 ± 0.02
$-Log_{10}(-T_2)$	6.215 ± 0.004	6.127 ± 0.004	6.113 ± 0.005	6.290 ± 0.003	6.369 ± 0.008	6.386 ± 0.007
$-Log_{10}(a_{L1})$	a)	2.47 ± 0.01	2.61 ± 0.02	a)	1.49 ± 0.01	1.22 ± 0.02
$-Log_{10}(a_{L2})$	1.38 ± 0.01	1.51 ± 0.01	1.61 ± 0.02	1.46 ± 0.01	1.56 ± 0.03	1.51 ± 0.03

a) not used; experimental artifacts (see text).

Table 1: Regression parameters and longitudinal dispersion lengths extracted from 5 experiments on two cores using the single–porosity transport model. BOMI69N and BOMI69Z refer to a single experiment in which break–through curves are measured with two different devices (see text). All units are those given in the text. Index 1 denotes the non–sorbing tracer and index 2 the sorbing tracer.

infiltration flow rate. BOMI60 was carried out with a higher infiltration flow rate than BOMI69. Activities of the tracers were measured using a lithium–drifted germanium γ–detector in all experiments. In the case of BOMI69, however, an additional sodium iodide γ–detector was used: BOMI69N refers to results obtained with the sodium iodide γ–detector and BOMI69Z to those obtained with the lithium–drifted γ–detector. In obtaining K_d, ϵ_p and ρ_p have been assigned the measured values for granodiorite at GTS: $2600 kgm^{-3}$ and 1% respectively [14].

The modelling of experiments BOMI58 and BOMI60 has been previously reported [3]. The dual–porosity model was fitted to the results for the sorbing tracer and S_2, T_2, U_2 and V_2 were obtained. The model was also fitted to the results for the non–sorbing tracer. However, as described in section 2, these experiments were carried out using apparatus which generated significant artifacts. Furthermore, the original design of the end–pieces did not allow the possibility of using a blank–run. Because of the shorter time–scale on which break–through of the non–sorbing tracer occurs, the processes of dispersion and matrix diffusion were masked by artifacts and, of the four regression parameters for the dual–porosity model S_1, T_1, U_1 and V_1 (the single–porosity model was not fitted), only T_1, the coefficient of the advection term for the non–sorbing tracer in equation (1), has been used in the present work. The remaining parameters, which are the coefficients of the dispersion and diffusion terms in equations (1) and (2), are unreliable. The physical parameters which can be obtained directly from these experiments are thus u, R_f and a_{L2} (equations (13-15)). To obtain estimates of the remaining physical parameters, U_1 and V_1 are also required (equations (16) and (19)). Therefore, for the two experiments BOMI58 and BOMI60, values of U_1 and V_1 are carried across from other experiments on the same core, which employed the modified apparatus: BOMI61 provides values of U_1 and V_1 for BOMI58 and BOMI69 provides values of U_1 and V_1 for BOMI60. It is therefore assumed here that the physical parameters on the left–hand sides of equations (17) and (19), while possibly dependent on the particular core used, are insensitive to the experimental conditions.

	core 1			*core 2*		
	BOMI58	**BOMI61**	**BOMI62**	**BOMI60**	**BOMI69N**	**BOMI69Z**
$-Log_{10}(S_1)$	a)	7.41 ± 0.01	7.63 ± 0.02	a)	6.45 ± 0.01	6.21 ± 0.03
$-Log_{10}(-T_1)$	4.82 ± 0.01	4.829 ± 0.004	4.814 ± 0.002	4.786 ± 0.005	4.956 ± 0.004	4.932 ± 0.007
$-Log_{10}(U_1)$	a)	4.89 ± 0.06	4.53 ± 0.03	a)	5.56 ± 0.09	5.18 ± 0.07
$-Log_{10}(V_1)$	a)	4.35 ± 0.06	3.94 ± 0.03	a)	4.12 ± 0.04	4.15 ± 0.09
$-Log_{10}(S_2)$	7.62 ± 0.01	7.69 ± 0.01	(—)	(7.758 ± 0.008)	(7.92 ± 0.02)	(7.91 ± 0.02)
	(7.62 ± 0.01)	(7.70 ± 0.01)				
$-Log_{10}(-T_2)$	6.200 ± 0.006	6.092 ± 0.008	(—)	(6.282 ± 0.004)	(6.368 ± 0.009)	(6.375 ± 0.008)
	(6.187 ± 0.008)	(6.087 ± 0.005)				
$-Log_{10}(U_2)$	6.35 ± 0.08	6.12 ± 0.05	—	—	—	—
$-Log_{10}(V_2)$	5.9 ± 0.2	5.8 ± 0.2	(—)	(5.39 ± 0.05)	(4.8 ± 0.8)	(5.1 ± 0.3)
	(5.9 ± 0.2)	(6.01 ± 0.09)				
$-Log_{10}(a_{L1})$	a)	2.58 ± 0.01	2.82 ± 0.02	a)	1.49 ± 0.01	1.28 ± 0.04
$-Log_{10}(a_{L2})$	1.42 ± 0.02	1.60 ± 0.02	(—)	(1.48 ± 0.01)	(1.55 ± 0.03)	(1.54 ± 0.03)
	(1.43 ± 0.02)	(1.61 ± 0.02)				

Table 2: Regression parameters and longitudinal dispersion lengths extracted using the dual–porosity transport model. Figures in parentheses are obtained by fixing $U_2 \equiv T_2 U_1 / T_1$ (see text).

		core 1			*core 2*		
		BOMI58	**BOMI61**	**BOMI62**	**BOMI60**	**BOMI69N**	**BOMI69Z**
u	$[ms^{-1}(\times 10^{-5})]$	—	1.40	1.43	—	1.09	1.13
a_{L1}	$[m(\times 10^{-3})]$	—	3.44	2.44	—	32.7	60.3
a_{L2}	$[m(\times 10^{-3})]$	42.51	30.8	24.8	34.6	27.6	30.9
R_f	[–]	24.7	18.7	20.0	31.9	25.4	27.5
σ_1^2	$[(\times 10^{-6})]$	—	6.83	18.6	—	2.69	4.99
σ_2^2	$[(\times 10^{-7})]$	4.92	4.91	8.74	1.53	12.5	8.08

Table 3: Physical parameters extracted from 5 experiments on two cores using the single–porosity transport model. The physical parameters are defined in the text. Index 1 denotes the non–sorbing tracer and index 2 the sorbing tracer.

		core 1			*core 2*		
		BOMI58	**BOMI61**	**BOMI62**	**BOMI60**	**BOMI69N**	**BOMI69Z**
u	$[m.s^{-1}(\times 10^{-5})]$	1.50	1.48	1.53	1.64	1.11	1.17
a_{L1}	$[m(\times 10^{-3})]$	—	2.64	1.53	—	32.0	53.0
a_{L2}	$[m(\times 10^{-3})]$	38.0	25.5	(—)	(34.2)	(27.8)	(29.5)
		(36.6)	(24.6)				
R_f	[–]	23.8	18.2	(—)	(31.6)	(25.8)	(27.7)
		(23.2)	(18.1)				
$\epsilon_p x_{max\ 1}/b$	$[(\times 10^{-2})]$	—	20.1	17.7	—	2.50	6.51
$\epsilon_p x_{max\ 2}/b$	$[(\times 10^{-2})]$	31.2	24.2	—	—	—	—
$\epsilon_p^2 D_p/b^2$	$[s^{-1}(\times 10^{-6})]$	—	2.59	5.22	—	0.069	0.428
$D_p/x_{max\ 1}^2$	$[s^{-1}(\times 10^{-5})]$	—	6.4	16.7	—	11.0	10.1
K_d	$[m^3 kg^{-1}(\times 10^{-4})]$	1.07	1.60	(—)	(0.46)	(0.29)	(0.50)
		(1.91)	(2.63)				
σ_1^2	$[(\times 10^{-6})]$	—	2.20	3.45	—	2.80	4.80
σ_2^2	$[(\times 10^{-7})]$	4.21	3.41	(—)	(1.53)	(12.4)	(8.11)
		(4.22)	(3.37)				

Table 4: Physical parameters extracted using the dual–porosity transport model. Figures in parentheses are obtained by fixing $U_2 \equiv T_2 U_1/T_1$ (see text).

Both models could be fitted to all the break–through curves for the non–sorbing tracer, although it should be noted that, in the case of BOMI69, the value of σ_1^2 is virtually identical for the two models (even showing a slightly higher value, and therefore a worse fit, for the dual–porosity model in the case of BOMI69N). Similarly, the single–porosity model could be fitted to all the break–through curves for the sorbing tracer. Only in the cases of BOMI58 and BOMI61, however, could a unique best–fit of the dual–porosity model to break–through curves for the sorbing tracer be obtained. For the remaining experimental results, the computer algorithm failed to find a minimum of χ_2^2 due to overparameterisation of the problem (see below): the dual–porosity model does fit the results, but, probably due to the amount of scatter in the measurements, the number of regression parameters is too large for *unique* best–fits to be found [15].

It can be seen from Table 4 that $\epsilon_p x_{max\ 1}/b$ and $\epsilon_p x_{max\ 2}/b$ take a similar value in the case of BOMI61 (the only experiment where both quantities can be extracted). On the assumption that this is generally true (i.e. that the thickness of the porous matrix is the same for both the sorbing and the non–sorbing tracer), the number of regression parameters which must be determined for the sorbing tracer with the dual–porosity model can be reduced from four to three. On setting $x_{max\ 1} = x_{max\ 2}$ in equations (18) and (19), a simplified model is obtained in which $U_2 \equiv T_2 U_1/T_1$ and hence $\rho_p K_d/\epsilon_p \simeq V_1/V_2$. Having reduced the number of regression parameters by one, the problem was no longer overparameterised and it was possible to fit this model to the break–through curves for the sorbing tracer in each of the experiments, with the exception of BOMI62. The extracted parameters from the fitting of the simplified model are presented in parentheses in table 2 and 4.

Contours of Log_{10}–concentration in the matrix for the non–sorbing and sorbing tracers are shown in fig.4 and fig.5 for experiment BOMI61 at different times during break–through. At early times, there is a negative gradient of concentration from the fracture into the porous matrix, resulting in diffusive flux out of the fracture. At later times ($\sim$ 1.5 *hours* in the case of the non–sorbing tracer and, although less pronounced, $\sim$ 10 *hours* in the case of the sorbing tracer), the concentration gradient and the direction of diffusive flux near to the fracture is reversed as the peak tracer concentration moves downstream.

Figs.6–11 show that the best fits to all the break–through curves for the sorbing tracer for both models yield very similar break–through curves, coinciding with each other at each measured time to within approximately the estimated standard deviation for the data (σ_2). Since the single–porosity model is a special case of the dual–porosity model, this demonstrates that overparameterisation accounts for the

failure to locate *unique* best–fits of the 4–parameter dual–porosity model for several of the experiments; in all cases apart from BOMI58 and BOMI61, no minimum for χ_2^2 could be located. Figs.8–11, showing those experiments for which the two models have been applied to the break–through curves of both tracers, demonstrate that the dual–porosity model more successfully reproduces the tailing part of the break–through curves for the non–sorbing tracer[7].

In order to test quantitatively whether the dual–porosity model gives a *significantly* better fit to the experimental data, the time dependence of the difference between the best–fits of the two models is calculated and compared with the magnitude of the experimental error. Only where the difference exceeds the experimental error is it meaningful to distinguish between the models. In order to obtain an estimate of the experimental errors, σ_1 and σ_2, the standard deviations of the data for non–sorbing and sorbing tracers respectively, are calculated from equation (12) (in using this equation, it is assumed that the dual–porosity model gives a good fit to the experimental break–through curves). The difference between the best–fits, denoted by $\delta C_1(L,t)$ and $\delta C_2(L,t)$ for the two tracers, are scaled by σ_1 and σ_2 respectively and plotted in fig.12. It can be seen that $\delta C_2(L,t)$ is not generally large with respect to experimental errors, never exceeding about $1.5\sigma_2$ for any of the experiments. $\delta C_1(L,t)$, however, takes higher values with respect to σ_1 (as high as $10\sigma_1$ for BOMI62). *The dual–porosity model thus significantly improves the goodness–of–fit to the break–through curves in the case of the non–sorbing tracer, but does not in the case of the sorbing tracer.*

This result is unexpected as matrix diffusion is more easily observed where the delay and consequent elongation in the tailing part of the break–through curve which it causes is assisted by sorption. Moreover, anions are often excluded from pores in the matrix which are small. However, figs.6–11 show that the scatter in the experimental measurements for the sorbing tracer is large in the tailing parts of the break–through curves when compared to that for the non–sorbing tracer[8], which may obscure the effect of matrix diffusion.

[7]For BOMI61, the tailing part of the break–through curve produced by the single–porosity model coincides closely with the blank–run and therefore represents only the effects of the apparatus. The dual–porosity model better reproduces the *additional* tailing produced by the rock core.

[8]the log–scale for the non–sorbing tracer would emphasise scatter

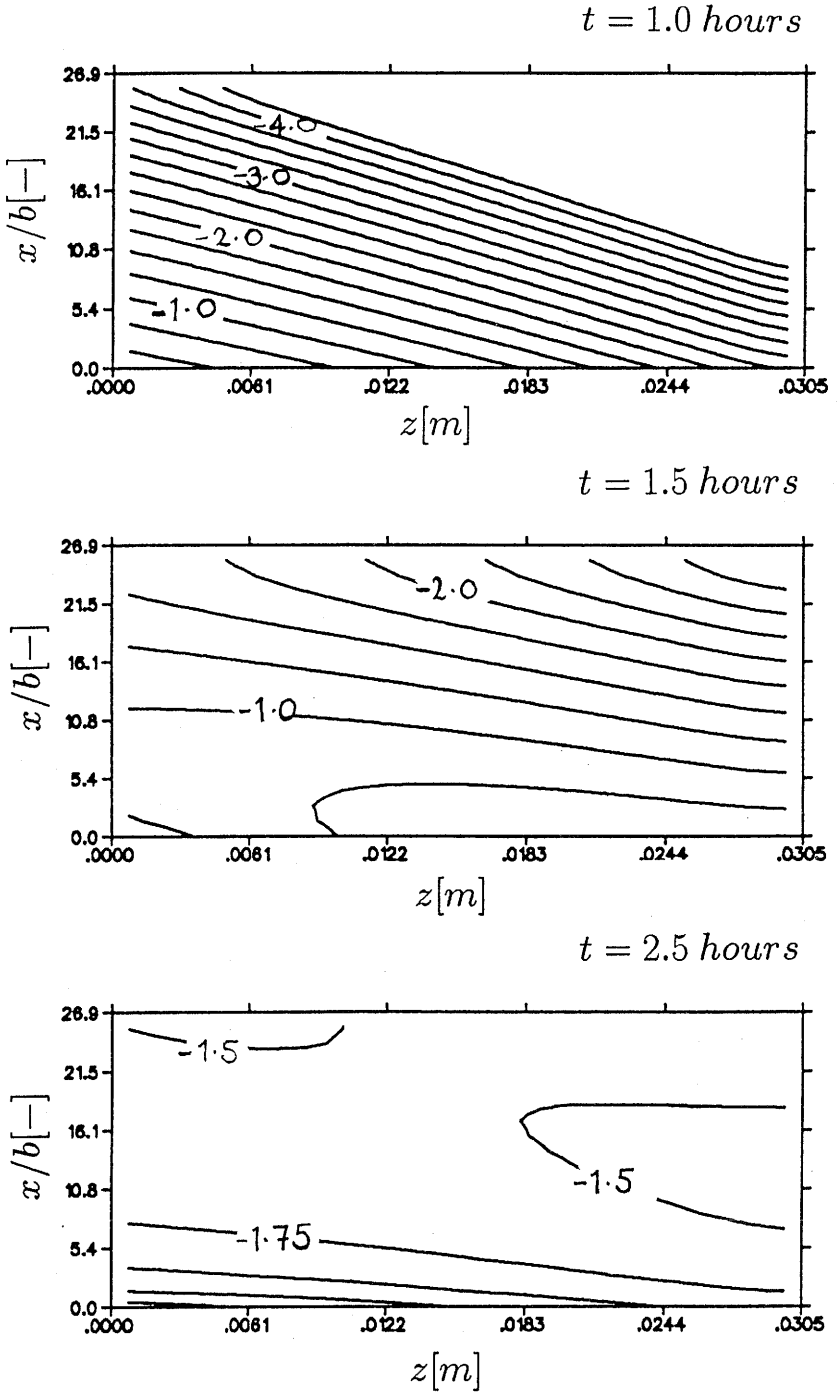

Figure 4. Infiltration experiment BOMI61: contours of ^{82}Br Log_{10}–concentration (relative to injection concentration) within the porous matrix at different times following injection. $x/b[-]$ is the ratio of distance into the porous matrix to the fracture half–aperture. $z[m]$ is the distance along the advection path.

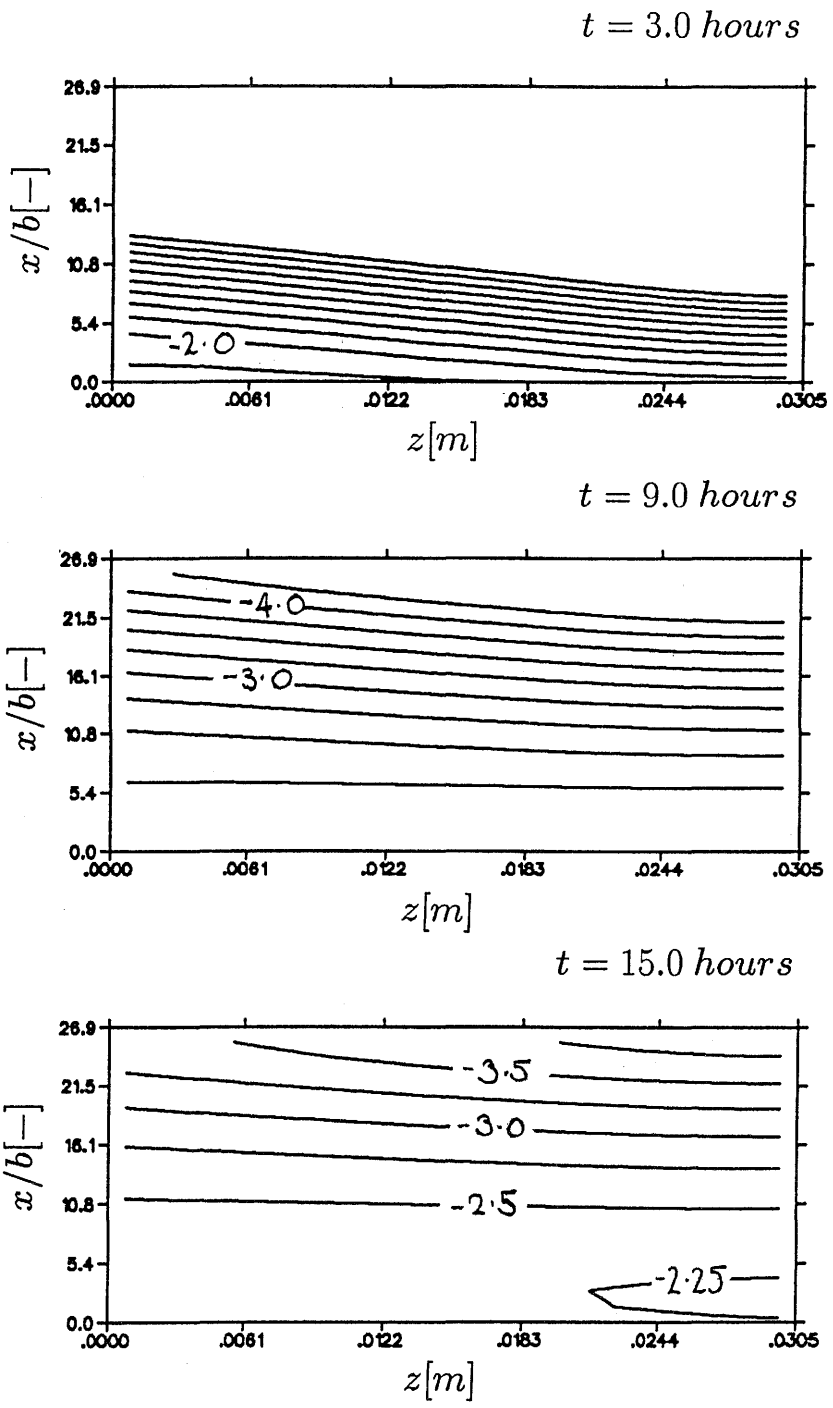

Figure 5. Infiltration experiment BOMI61: contours of ^{24}Na Log_{10}–concentration (relative to injection concentration) within the porous matrix at different times following injection.

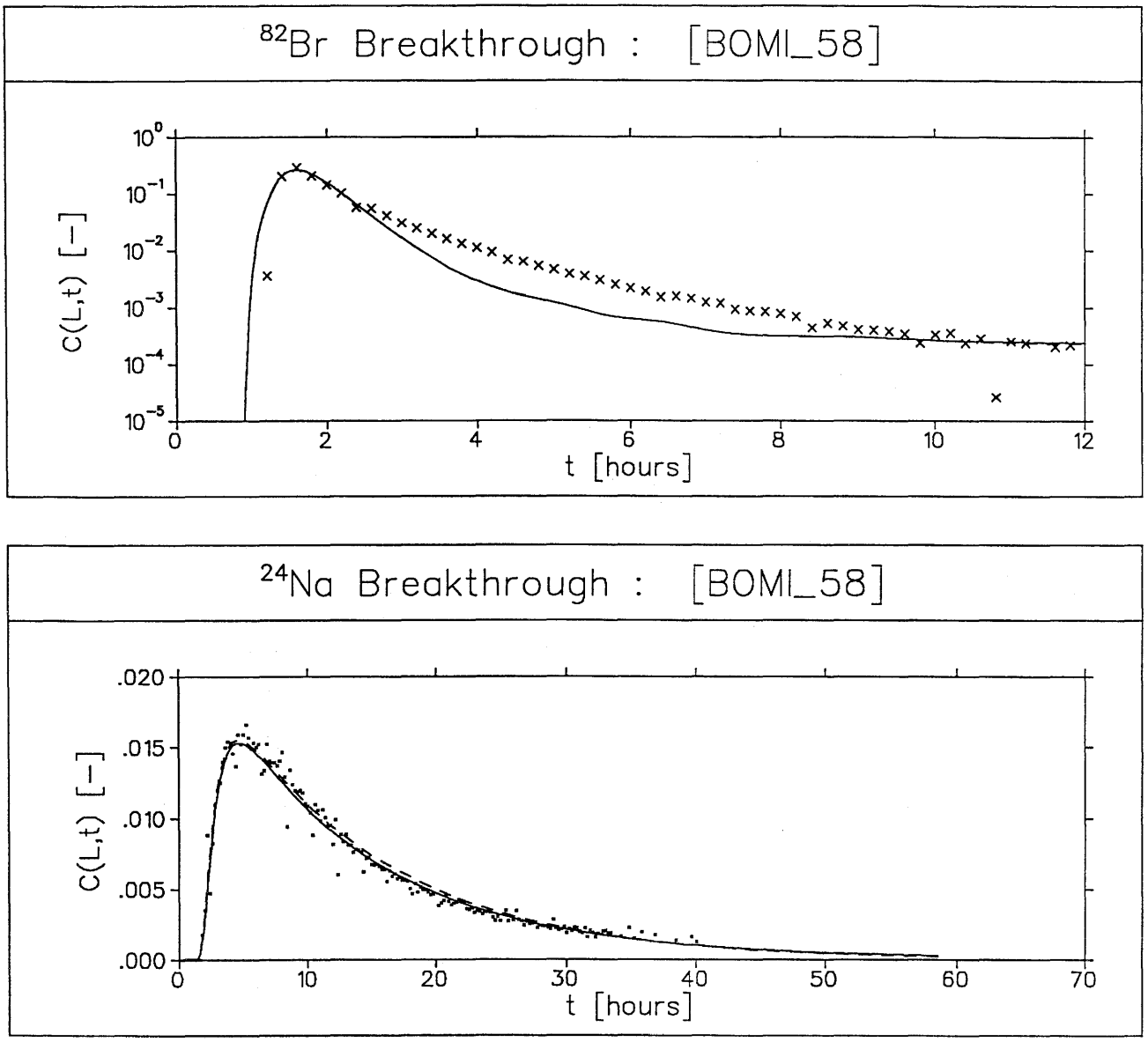

Figure 6. Infiltration experiment BOMI58: experimental data and models fitted to ^{82}Br and ^{24}Na break–through curves. Concentration normalised to that of the injected pulse. Single–porosity model not fitted to ^{82}Br break–through (see text).

× × × experimental data - break–through curves

- - - - single-porosity model

——— dual-porosity model.

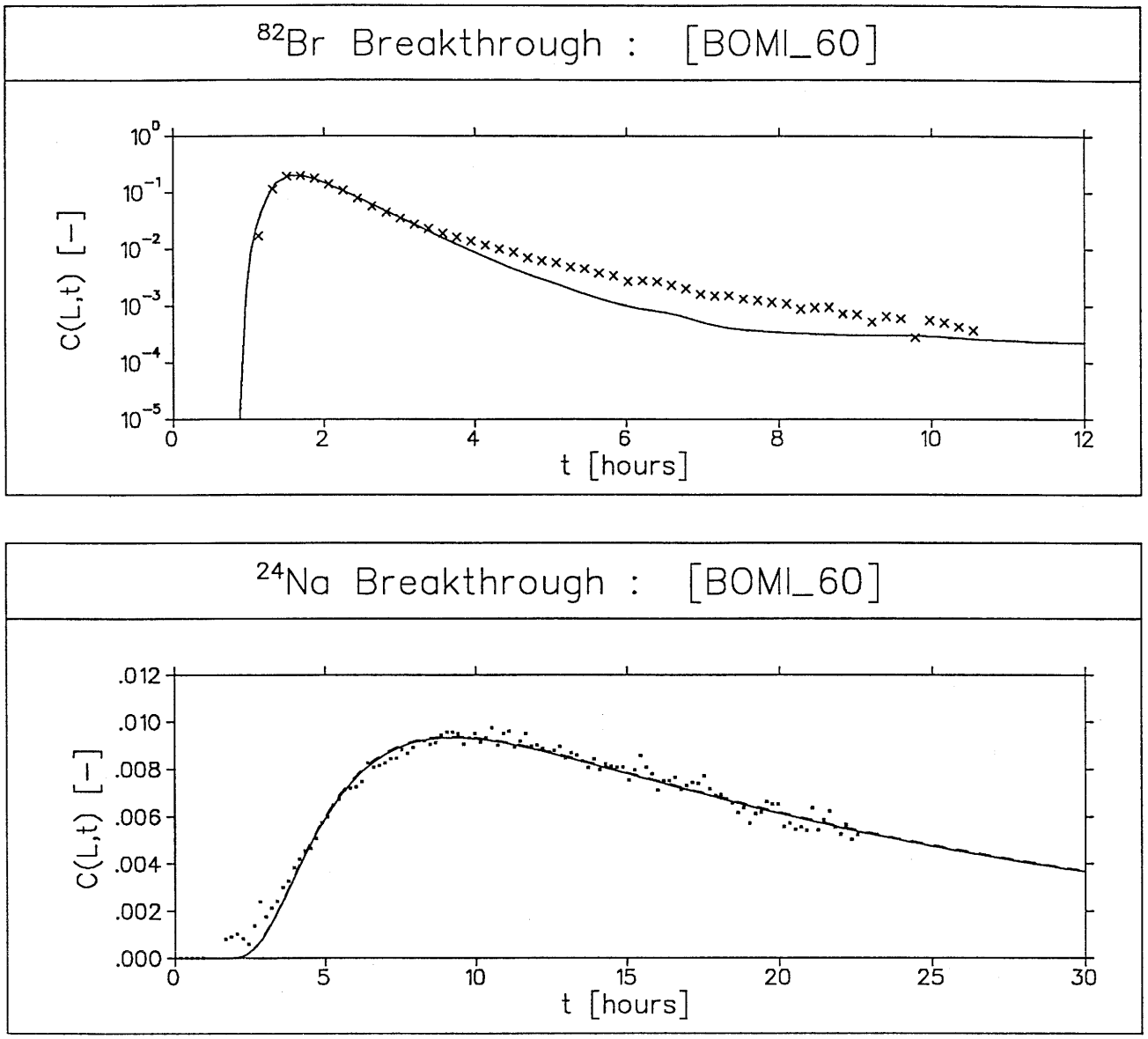

Figure 7. Infiltration experiment BOMI60: experimental data and models fitted to ^{82}Br and ^{24}Na break–through curves. Single–porosity model not fitted to ^{82}Br break–through (see text).

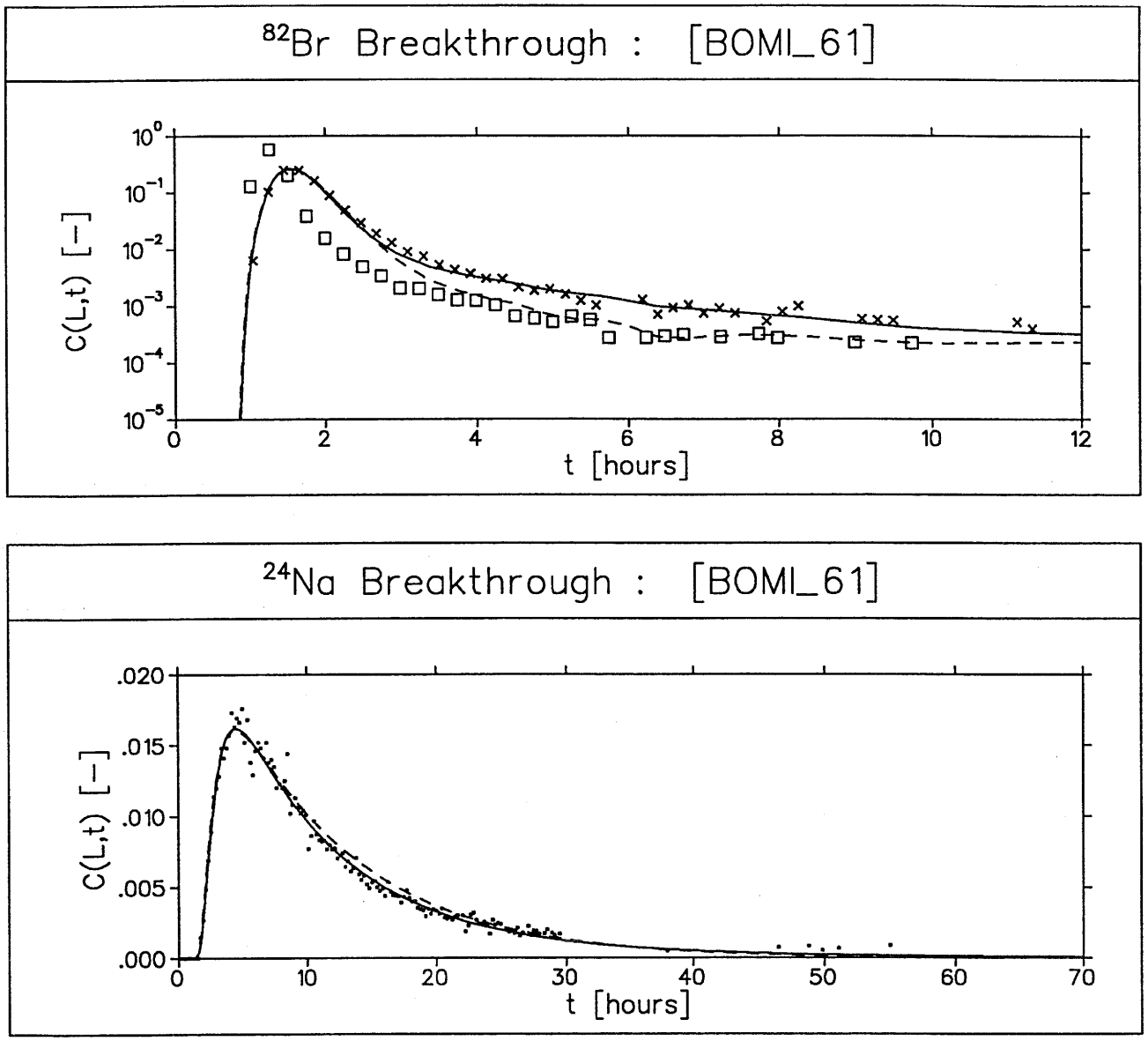

Figure 8. Infiltration experiment BOMI61: experimental data and models fitted to ^{82}Br and ^{24}Na break–through curves. A blank–run gives the initial form of the tracer pulse on entry into the core.
□ □ □ □ experimental data - blank–run

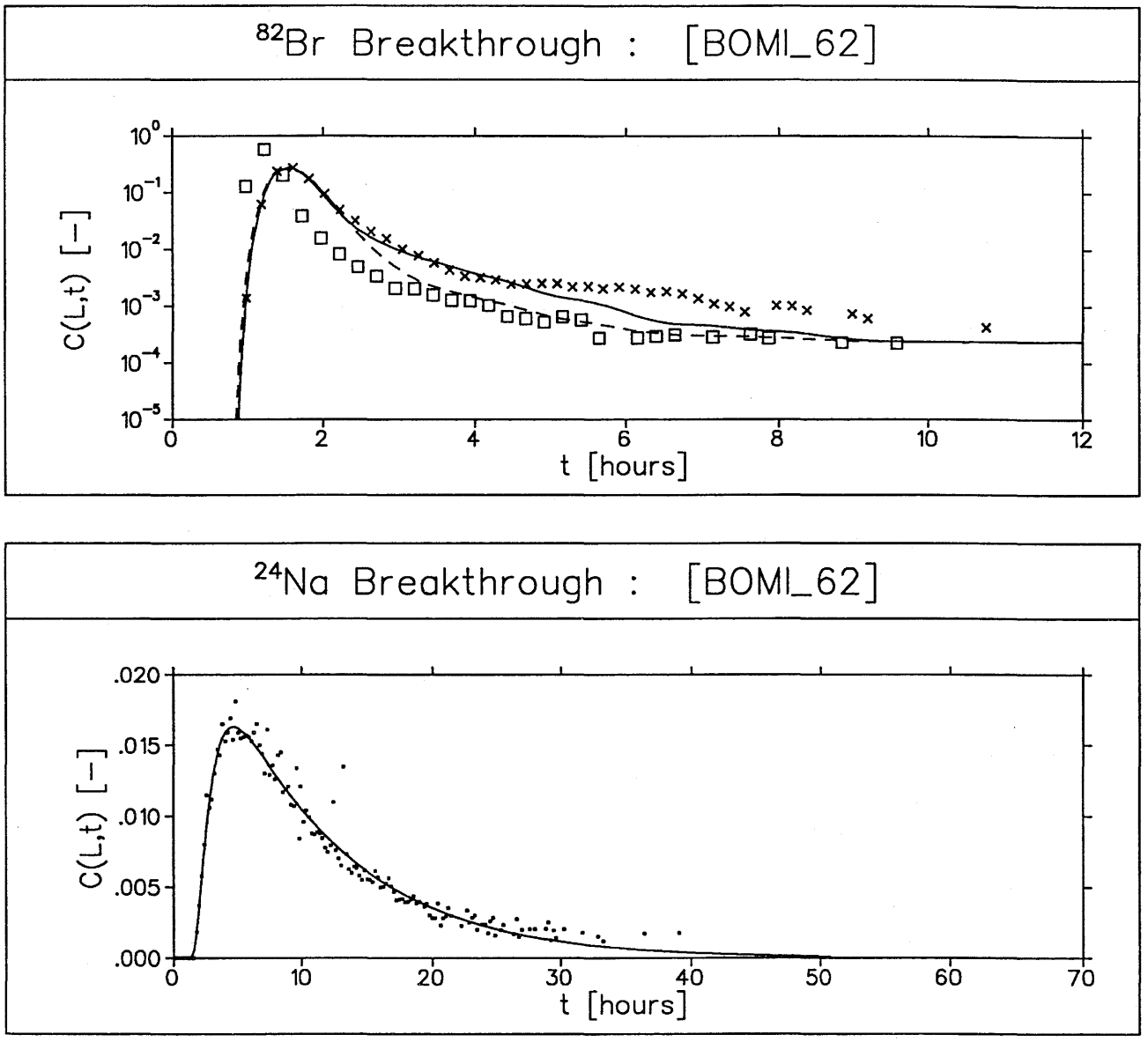

Figure 9. Infiltration experiment BOMI62: experimental data and models fitted to ^{82}Br and ^{24}Na break–through curves.

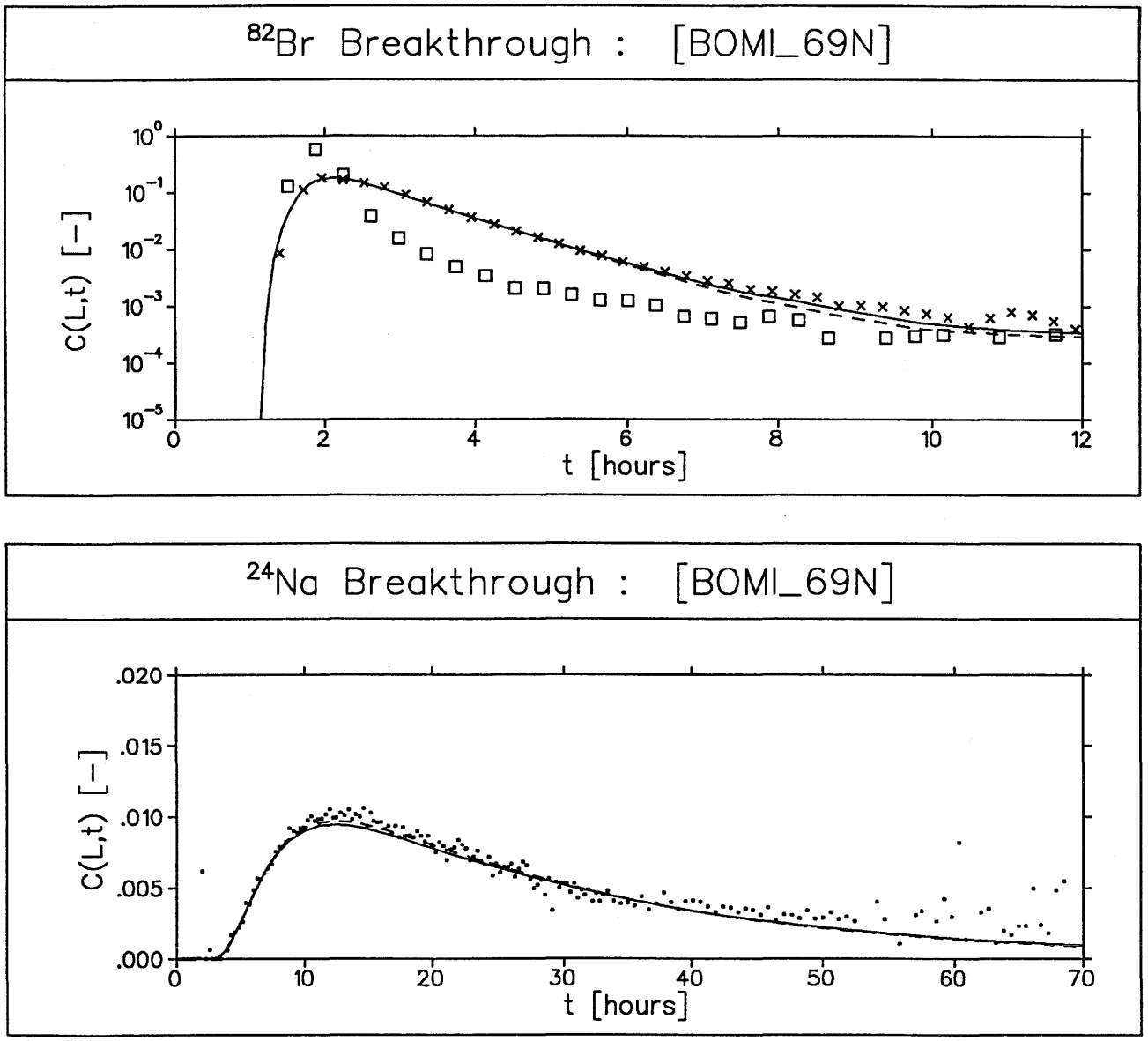

Figure 10. Infiltration experiment BOMI69N: experimental data and models fitted to ^{82}Br and ^{24}Na break–through curves.

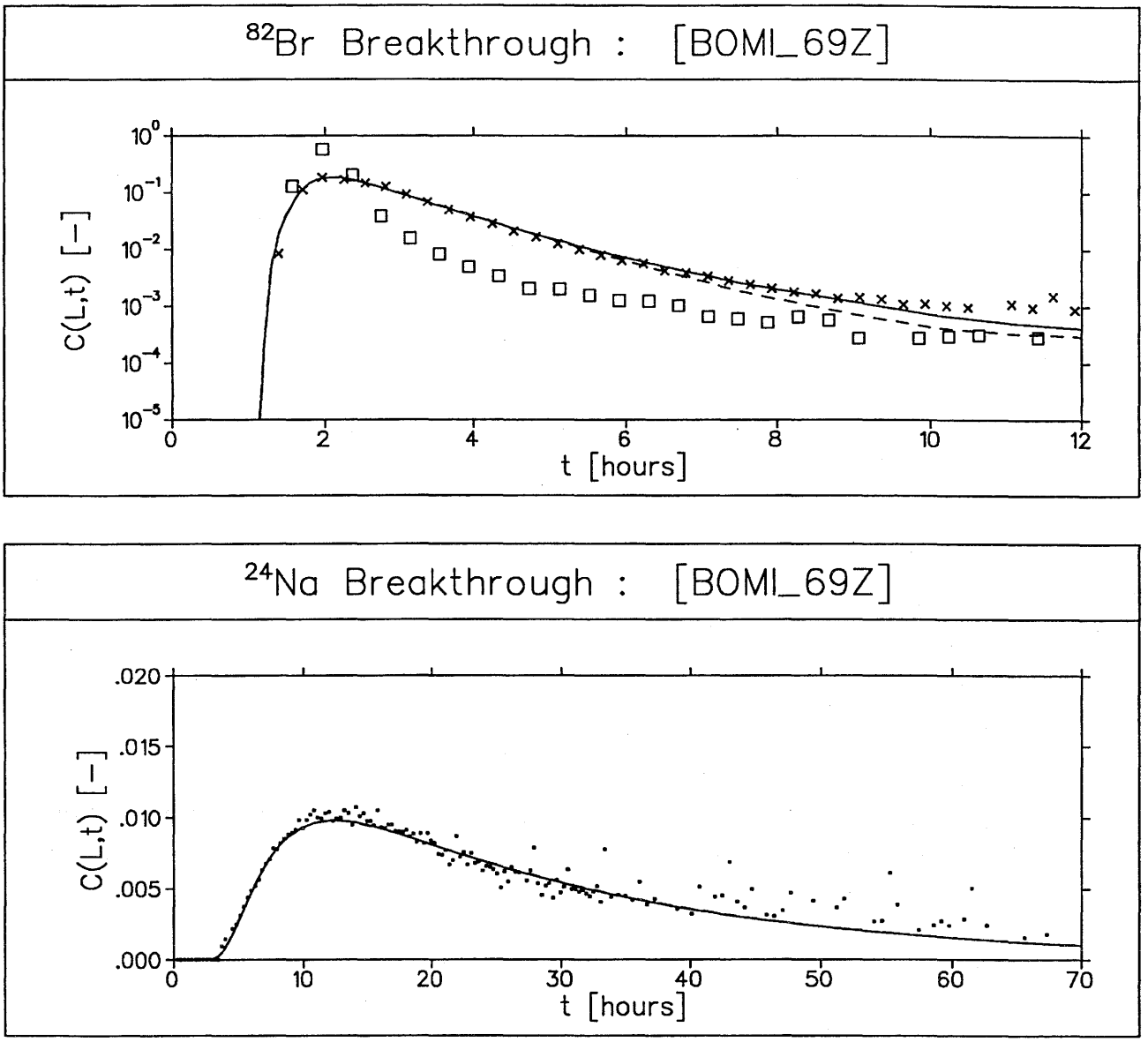

Figure 11. Infiltration experiment BOMI69Z: experimental data and models fitted to ^{82}Br and ^{24}Na break–through curves.

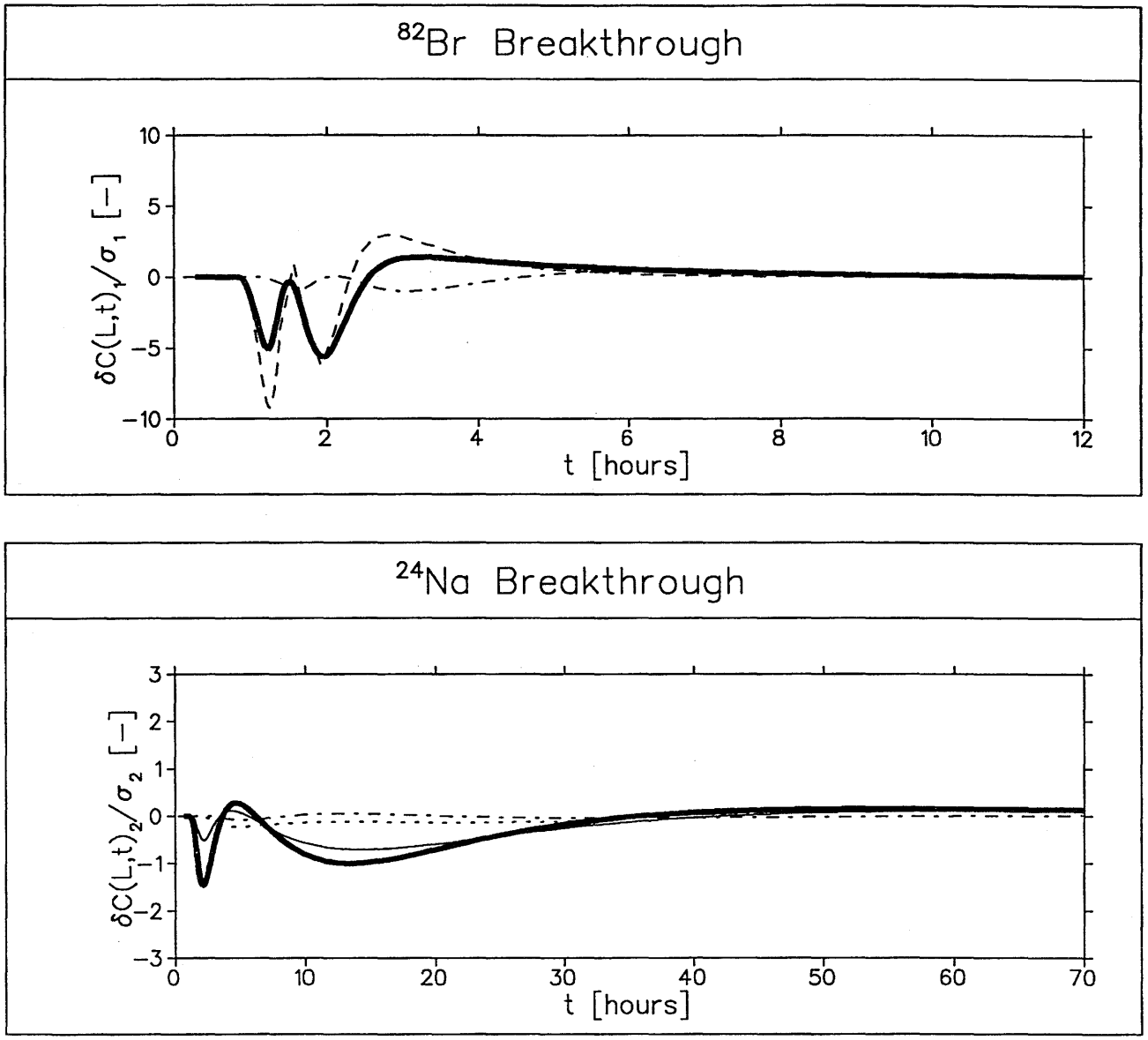

Figure 12. Time development of difference between the best–fits to the break–through curves obtained respectively with the single–porosity and dual–porosity models. σ_1 and σ_2 are standard deviations giving a measure of the uncertainty in the experimental data for the non–sorbing and sorbing tracer respectively.
____ BOMI58, - - - - BOMI60, ____ BOMI61, — — — — BOMI62, — - — - — - BOMI69Z.

5 Discussion of Parameter Values

To summarize, single and dual–porosity transport models have been fitted to the break–through curves from two–tracer, high–pressure infiltration experiments on two different rock cores. On the basis of this work alone, it is not possible to demonstrate that the dual–porosity model is more appropriate for the sorbing tracer or that either model provides a *good fit* to the experimental data. However, *assuming the fits to be good*, several physical parameters (or combinations of parameters) are determined. Confidence in the modelling approach is enhanced by demonstrating that the parameter values are reasonable by comparison with independent experiments.

The physical parameters which can be determined using either model are the velocity of the infiltration fluid (u), the surface–based retardation factor (R_f) and longitudinal dispersion length for both tracers (a_{L1} and a_{L2}). For all experiments, u was found to be in the order of $10^{-5} ms^{-1}$ and R_f to lie within the relatively narrow range of 18 to 32. R_f, which represents sorption on the fracture walls, may be written as

$$R_f = 1 + \frac{1}{b} K_a \tag{20}$$

where $K_a[m]$ is a surface–based distribution constant. Assuming that the mineralogy (and therefore chemistry) of the fracture walls is similar for the two cores, giving similar values for K_a, equation (20) suggests that the aperture half–width b is also similar.

a_{L2} lies in the range $2cm$ to $4cm$ for both cores. The range of values of a_{L1} for core 2, between $3cm$ and $6cm$, is similar to that of a_{L2}. For core 1, however, a_{L1} is an order of magnitude smaller: between $1.5mm$ and $3.5mm$. Table 1 and table 2 give values for the logarithms of a_{L1} and a_{L2}, together with standard deviations in these values. They show that the low values of a_{L1} for core 1 are not explained by uncertainty in the best–fit due to random experimental error. The origin of the dispersion process lies in the heterogeneous properties of the fracture, which give rise to microscopic flow paths with differing tracer transit times. The magnitude of a_L is dictated by the length scales of inhomogeneities both in tracer–independent quantities, such as fracture aperture, and in tracer dependent quantities such as sorption along the flow path [16]. Different longitudinal dispersion lengths for non–sorbing and sorbing tracers are, therefore, to be expected if it is variability in sorption which determines a_L for sorbing tracers. For porous media, there have been studies which suggest that longitudinal dispersion is not constant, but depends on the mean transport distance, approaching an asymptotic value dependent on the statistical

properties of the medium. The *scale effect* is reviewed in [17]. The difference between the two cores may indicate that they are not sufficiently large to provide a REV (representative elementary volume). This could be tested by carrying out further experiments with cores of different length.

Physical parameters which can be determined from the dual–porosity model alone are the thickness of the porous matrix for both tracers with respect to the fracture half–aperture ($\epsilon_p x_{max\ 1}/b$ and $\epsilon_p x_{max\ 2}/b$), the ratio of the diffusion coefficient to the square of the fracture half–aperture ($\epsilon_p^2 D_p/b^2$) and the distribution constant for the sorbing tracer (K_d). The quantities $\epsilon_p x_{max\ 1}/b$ and $\epsilon_p^2 D_p/b^2$, both derived by fitting the dual–porosity model to the break–through curves for the non–sorbing tracer, each differ by one to two orders of magnitude between the two cores. Eliminating ϵ_p/b from these two quantities, values of $D_p/x_{max\ 1}^2$ are obtained, also given in Table 2, which show relatively little variability, taking values in the order of $10^{-4}s^{-1}$ for both cores. This implies that it is ϵ_p/b, the ratio of matrix porosity to fracture aperture, which is chiefly responsible for the differences between the two cores. As discussed above, however, lack of variability in R_f suggests that suggests that the aperture is similar in both cases. This leaves only matrix porosity to account for the differences, with core 2 having the lower value of ϵ_p.

Although it is not possible to obtain values of the fracture half–aperture width b directly from the fitting procedure, b can be estimated from $\epsilon_p^2 D_p/b^2$ by assuming reasonable values for $\epsilon_p D_p$ and ϵ_p. The effective diffusion coefficient can be written

$$\epsilon_p D_p = k\epsilon_p D_0 \tag{21}$$

where D_0 is the diffusion coefficient in free water ($\sim 10^{-9}m^2s^{-1}$ for the major ions found in groundwater). Values of k between about 0.01 and 0.5 are commonly observed in diffusion experiments for non–sorbing ions in porous geological materials [18]. Taking $\epsilon_p = 1\%$ [14], ranges of values for b of $14 - 140\mu m$ for core 1 and $48 - 850\mu m$ for core 2 are obtained.

Fitted values of K_d for the sorbing tracer lie in the range $1 - 3 \times 10^{-4}m^3kg^{-1}$ for core 1 and $3 - 5 \times 10^{-5}m^3kg^{-1}$ for core 2. In the case of core 2, however, σ_2^2, and thus the merit function for the best fit $\chi^2_{min\ 2}$, is virtually identical for single–porosity and dual–porosity models. An examination of the variation of a relative merit function with K_d for each of the experiments demonstrates the reason for this (fig.13). The relative merit function is defined here as $\chi_2^2/\chi^2_{min\ 2}$. It has a well–defined minimum for the experiments BOMI58 and BOMI61 (core 1), whereas, for the experiments BOMI60 and BOMI69 (core 2), the function is almost flat for K_d, where $K_d < 10^{-4}m^3kg^{-1}$. A wide range of K_d values give fits of the same quality,

so the single–porosity model, which corresponds to the particular choice of $K_d = 0$, gives almost as good a fit as the higher values of K_d. Where there is no well defined minimum, no reliable value for K_d can be given and the calculated values of K_d for core 2 are therefore excluded. Values of K_d for the sorption of Na on Grimsel fracture material obtained from independent experiments are compared with the range of values for core 1 in the present work below:

$1 - 3 \times 10^{-4} m^3 kg^{-1}$ [Present Work].

$0.5 - 2.5 \times 10^{-4} m^3 kg^{-1}$ [19].

$3 \times 10^{-4} m^3 kg^{-1}$ [5].

$20 \times 10^{-4} m^3 kg^{-1}$ [6].

The range of values in [19] was calculated from the results of a geochemical field experiment together with an ion exchange model and that of [5] from field migration experiments together with the dual–porosity transport model. The value in [6] was measured directly in laboratory batch–sorption experiments. Agreement of the present work with the calculated values from both field experiments is good. Laboratory batch sorption experiments give a K_d which is an order of magnitude larger. These experiments, however, were performed on crushed material in order to obtain results within a reasonable time. The crushing process is likely to have disrupted the structure of the rock and to have created fresh surfaces on which nuclides may sorb, thus yielding a larger value for K_d. A slight difference in water chemistry may also have been important.

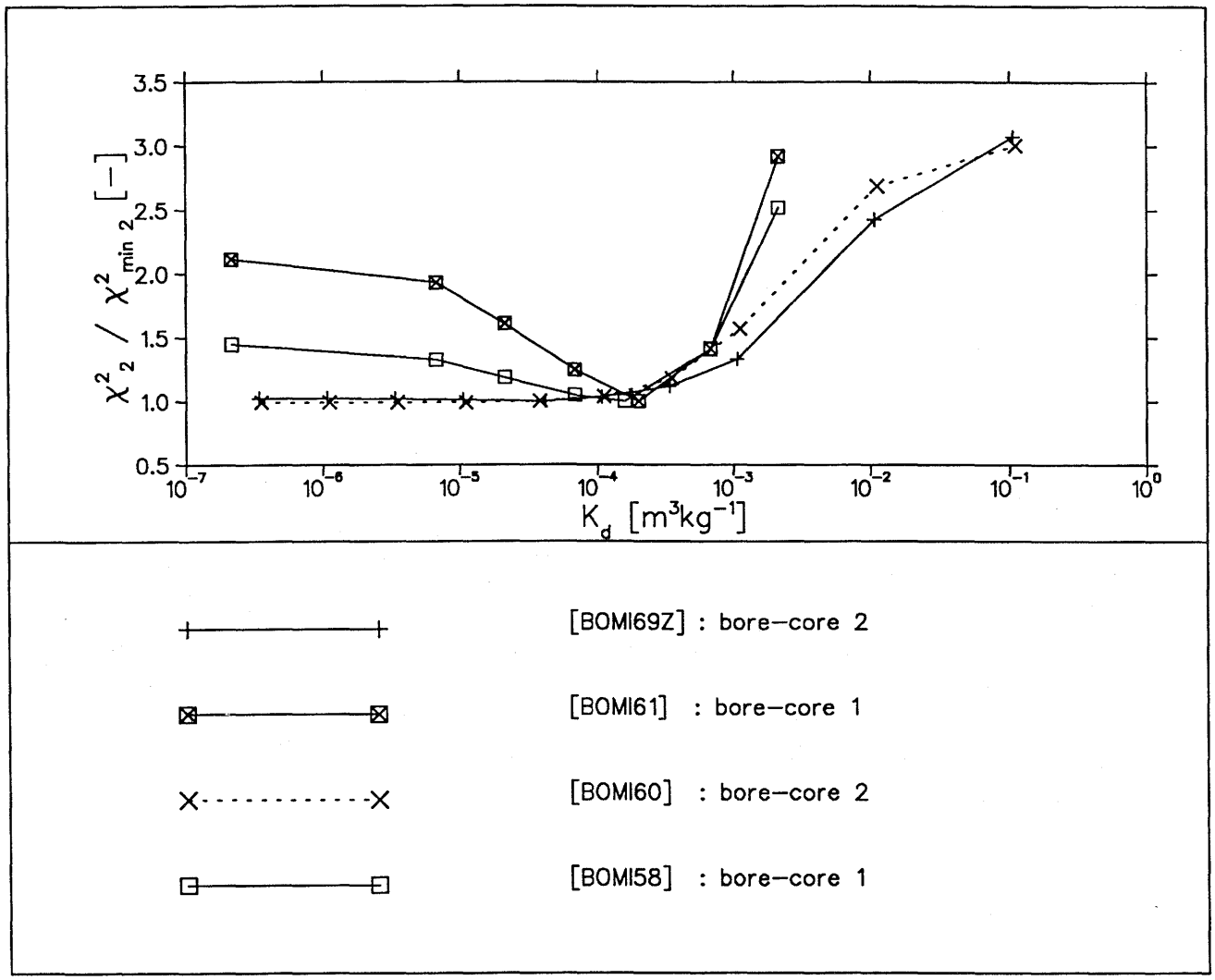

Figure 13 Variation of relative merit function, a measure of goodness–of–fit relative to the best–fit (defined in the text), with the distribution constant for the sorbing tracer $K_d[m^3kg^{-1}]$.

6 Conclusions

- The dual–porosity model is able to reproduce the tailing part of the break–through curves for the non–sorbing tracer, whereas the single–porosity model is not.
- The single–porosity model and dual–porosity model both reproduce the break–through curves for the sorbing tracer to within the estimated errors for most of the experiments. However, the effect of matrix diffusion may be obscured by scatter in the experimental measurements, which is larger than for the non–sorbing tracer in the tailing parts of the break–through curves.
- For most experiments, fitting of the four–parameter dual–porosity model to the break–through curves for the sorbing tracer is not possible due to overparameterisation. In order to obtain a unique best–fit, it is necessary to reduce the number of regression parameters, which can be achieved by making the reasonable assumption that thickness of the porous matrix is the same for both tracers.
- The longitudinal dispersion length is generally in the order of a few centimetres. A smaller longitudinal dispersion length was found for one of the cores in the case of the non–sorbing tracer. This is at present unexplained; the tracer–dependence of the dispersion process should be investigated in further experiments, as should the dependence on core length.
- A comparison of the values of R_f, $\epsilon_p x_{max}/b$ and $\epsilon_p^2 D_p/b^2$ for the two cores suggests that the mean aperture width is similar, whereas the matrix porosity varies between the cores.
- A physically plausible range of values for the mean aperture b has been extracted.
- The extracted range of values for K_d agrees well with those calculated from the results of two separate field experiments. Direct measurement of K_d in laboratory batch–sorption experiments gives a larger value, but this difference may be explained by the larger surface area available for sorption.
- In future experiments, it would be desirable to replace the downstream end–piece with a design giving negligible dispersion effects. This would make the assumption that transport processes within the end–piece and the sample can be interchanged unnecessary. Such a design, first proposed by M.Bradbury (PSI) and described in [10], involves a continuous flushing of the end–piece, thus greatly reducing the residence time of the tracer.

References

[1] SKI (1987) *INTRAVAL Project Proposal*, SKI 87:3, Swedish Nuclear Power Inspectorate, Stockholm, Sweden.

[2] A.Jakob and J.Hadermann (1990) *INTRAVAL test case 1b–modelling results.* PSI–Report Nr.105, PSI, Würenlingen and Villigen and Nagra NTB 91–27, Nagra, Baden.

[3] P.A.Smith, J.Hadermann and K.Bischoff (1990) *Dual porosity modelling of infiltration experiments on fractured granite.* GEOVAL'90 conference, May 14–17, Stockholm, Sweden.

[4] J.Hadermann and F.Roesel (1985) *Radionuclide chain transport in inhomogeneous crystalline rocks. Limited matrix diffusion and effective surface sorption.* EIR–Report Nr. 551, PSI, Würenlingen and Villigen and Nagra NTB 85–40, Nagra, Baden.

[5] F.Herzog (1991) *A simple transport model for the Grimsel migration experiment.* PSI–report Nr.106, PSI, Würenlingen and Villigen.

[6] S.Aksoyoglu, C.Bajo and M.Mantovani (1990) *Batch sorption experiments with iodine, bromine, strontium and cesium on Grimsel mylonite*, PSI–Report Nr.83, PSI, Würenlingen and Villigen and Nagra NTB–91–06, Nagra, Baden.

[7] K.Bischoff (1990), Private communication.

[8] K.Bischoff, K.Wolf and B.Heimgartner (1987) *Hydraulische Leitfähigkeit, Porosität und Uranrückhaltung von Kristallin und Mergel: Bohrkern–Infiltrationsversuche.* EIR–Report Nr. 628, PSI, Würenlingen and Villigen.

[9] Programm Entsorgung (1989) *Laboratory investigations in support of the migration experiments at the Grimsel test site.* Edited by M.Bradbury. PSI–Report Nr. 28, PSI, Würenlingen and Villigen and Nagra NTB 88–23, Nagra, Baden.

[10] P.A.Smith and W.R.Alexander (1990) *Proposed Experimental Programme for the High–Pressure Infiltration Apparatus.* AN–41–90–25, PES–90–525, PSI, Würenlingen and Villigen.

[11] J.Carerra (1991), Private communication.

[12] A.Jakob, J.Hadermann and F.Roesel (1989) *Radionuclide chain transport with matrix diffusion and non–linear sorption.* PSI–Report Nr.54, PSI, Würenlingen and Villigen and Nagra NTB 90–13, Baden.

[13] D.W.Marquardt (1963) J.Soc.Ind.Appl.Math., 11, 431–441.

[14] P.Bossart and M.Mazurek (1990) *Strukturgeologische Charakterisierung und Geometrie der Wasser–Fliesswege in der Migrationsscherzone VT 420, Felslabor Grimsel.* Nagra NIB 90–44, Nagra, Baden.

[15] W.W–G.Yeh (1986) *Review of parameter identification procedures in groundwater hydrology: the inverse problem.* Water Resour. Res., 22, 95–108.

[16] L.W.Gelhar (1987) *Applications of stochastic models to solute transport in fractured rocks.* SKB Technical Report 87–05, SKB, Stockholm, Sweden.

[17] J.F.Pickens and G.E.Grisak (1981) *Scale–dependent dispersion in a stratified granular aquifer.* Water Resour. Res., 17, 1191–1211.

[18] R.A.Freeze and J.A.Cherry: *Groundwater.* Prentice–Hall Inc., Eagle Cliffs, N.J.,1979.

[19] J.Eikenberg, B.Baeyens and M.Bradbury (1990) *The Grimsel migration experiment: a hydrogeochemical equilibrium test.* PSI–Report (in press), PSI, Würenlingen and Villigen and Nagra NTB–90–39, Nagra, Baden.

Acknowledgements

Special thanks are due to K.Bischoff (PSI) for providing the experimental results prior to publication. Several colleagues have contributed to this work through helpful discussion, in particular W.R.Alexander (University of Berne), U.Frick (Nagra), M.Bradbury, J.Hadermann, W.Heer, A.Jakob and T.Karapiperis (all PSI). Partial financial support by Nagra is gratefully acknowledged.